Constraints from 210 Pb and 7 Be on wet deposition and transport in a global three-dimensional chemical tracer model driven by assimilated meteorological fields

JOURNAL OF GEOPHYSICAL RESEARCH, VOL. 106, NO. D11, PAGES 12,109–12,128, JUNE 16, 2001

Constraints from ^{210}Pb and ^{7}Be on wet deposition and transport in a global three-dimensional chemical tracer model driven by assimilated meteorological fields

Hongyu Liu, Daniel J. Jacob, Isabelle Bey, and Robert M. Yantosca

Department of Earth and Planetary Sciences and Division of Engineering and Applied Sciences, Harvard University, Cambridge, Massachusetts

Abstract. The atmospheric distributions of the aerosol tracers ^{210}Pb and ^{7}Be are simulated with a global three-dimensional model driven by assimilated meteorological observations for 1991–1996 from the NASA Goddard Earth Observing System (GEOS1). The combination of terrigenic ^{210}Pb and cosmogenic ^{7}Be provides a sensitive test of wet deposition and vertical transport in the model. Our simulation of moist transport and removal includes scavenging in wet convective updrafts (40% scavenging efficiency per kilometer of updraft), midlevel entrainment and detrainment, first-order rainout and washout from both convective anvils and large-scale precipitation, and cirrus precipitation. Observations from surface sites in specific years are compared to model results for the corresponding meteorological years, and observations from aircraft missions over the Pacific are compared to model results for the days of the flights. Initial simulation of ^{7}Be showed that cross-tropopause transport in the GEOS1 meteorological fields is too fast by a factor of 3–4. We adjusted the stratospheric ^{7}Be source to correct the tropospheric simulation. Including this correction, we find that the model gives a good simulation of observed ^{210}Pb and ^{7}Be concentrations and deposition fluxes at surface sites worldwide, with no significant global bias and with significant success in reproducing the observed latitudinal and seasonal distributions. We achieve several improvements over previous models; in particular, we reproduce the observed ^{7}Be minimum in the tropics and show that its simulation is sensitive to rainout from convective anvils. Comparisons with aircraft observations up to 12-km altitude suggest that cirrus precipitation could be important for explaining the low concentrations in the middle and upper troposphere.

1. Introduction

The radiative forcing by anthropogenic aerosols is a major uncertainty in current assessments of climate change [*Intergovernmental Panel on Climate Change (IPCC)*, 2000]. Climate models must resolve the spatial heterogeneity of aerosols and the coupling to the hydrological cycle arising from the short lifetime of aerosols against wet deposition [*Koch et al.*, 1999; *Kiehl et al.*, 2000]. Better simulation of aerosol deposition in global models is needed [*Penner et al.*, 1994]. We address this issue here by simulation of the aerosol tracers ^{210}Pb and ^{7}Be in a global three-dimensional (3-D) chemical tracer model (GEOS-CHEM) driven by assimilated meteorological observations from the Goddard Earth Observing System data assimilation system (GEOS1 DAS) at the NASA Data Assimilation Office (DAO) [*Schubert et al.*, 1993; *Allen et al.*, 1996b]. Simulation of both ^{210}Pb and ^{7}Be in a model driven by assimilated meteorological data provides improved constraints for testing aerosol deposition schemes by comparison with atmospheric observations, including vertical profiles measured from aircraft.

Terrigenic ^{210}Pb (half-life 22.3 years) is the decay daughter of ^{222}Rn (half-life 3.8 days) emitted from the continental crust. Cosmogenic ^{7}Be (half-life 53.3 days) is produced by cosmic ray spallation reactions in the stratosphere and upper troposphere [*Lal et al.*, 1958]. Both ^{210}Pb and ^{7}Be attach quickly and indiscriminately to available aerosols [*Maenhaut et al.*, 1979; *Sanak et al.*, 1981; *Bondietti et al.*, 1987, 1988]. The fate of ^{210}Pb and ^{7}Be then becomes that of those aerosols, which move with the air flow until scavenged by precipitation or deposited to the surface.

Because of their contrasting sources at low and high altitudes, ^{210}Pb and ^{7}Be are a useful pair for testing

Paper number 2000JD900839.
0148-0227/01/2000JD900839$09.00

wet deposition processes in a global 3-D atmospheric model. Long-term data records of ^{210}Pb [*Preiss et al.*, 1996] and ^{7}Be [*Feely et al.*, 1989; *Larsen et al.*, 1995] are available from worldwide networks, providing good constraints for model validation. Beyond wet deposition, simulation of ^{210}Pb and ^{7}Be in a global model tests the ability of the model to describe transport of continental air over the oceans [*Turekian et al.*, 1989; *Balkanski et al.*, 1993, hereafter referred to as B93], transport from the stratosphere [*Rangarajan and Gopalakrishnan*, 1970; *Viezee and Singh*, 1980; *Sanak et al.*, 1985; *Dibb et al.*, 1992, 1994; *Rehfeld and Heimann*, 1995], and subsidence in the troposphere [*Feely et al.*, 1989; *Koch et al.*, 1996, hereafter referred to as K96].

Global 3-D simulations of ^{210}Pb and ^{7}Be have been conducted by a number of investigators. *Feichter et al.* [1991] and *Brost et al.* [1991] used a tracer model driven by the European Centre for Medium Range Weather Forecasting (ECMWF) meteorological fields. A first-order rainout scheme [*Giorgi and Chameides*, 1986, hereafter referred to as GC86] was used to compute wet scavenging. The model overestimated surface ^{210}Pb concentrations by 40% while producing better results for ^{7}Be. The overestimate of ^{210}Pb was attributed to insufficient aerosol scavenging in convective updrafts. The observed tropical minimum in surface ^{7}Be concentrations [*Viezee and Singh*, 1980; *Uematsu et al.*, 1994] was not captured. Using the ECMWF model and a first-order scavenging parameterization developed by *Kasibhatla et al.* [1991], *Rehfeld and Heimann* [1995] simulated the distributions of ^{210}Pb, ^{7}Be, ^{10}Be and ^{90}Sr with a focus on the use of the concentration ratio ^{10}Be/^{7}Be as an indicator of stratosphere-troposphere exchange. They were more successful at reproducing the tropical minimum in surface ^{7}Be concentrations.

B93 and K96 simulated the global distributions of ^{210}Pb and ^{7}Be, respectively, using a general circulation model (GCM) developed at the Goddard Institute for Space Studies (GISS). They computed scavenging by convective precipitation as part of the wet convective mass transport, instead of separately as a first-order rainout loss. Coupling of scavenging and convective transport greatly improved the ^{210}Pb simulation relative to that of *Feichter et al.* [1991]. However, K96 found that surface ^{7}Be concentrations in the tropics were overestimated, which they attributed to lack of entrainment in the GCM convection scheme.

A few additional studies have intercompared different wet precipitation scavenging schemes using ^{210}Pb [*Lee and Feichter*, 1995; *Guelle et al.*, 1998a; *Giannakopoulos et al.*, 1999]. In the World Climate Research Programme (WCRP) model intercomparison workshop of 1995, various deposition schemes employed in different global models were intercompared using ^{210}Pb and SO_x(SO_2, SO_4^{2-}) [*Rasch et al.*, 2000]. It was found that many 3-D transport models differ considerably in the simulation of ^{210}Pb although they produce similar distributions of ^{222}Rn.

We present in this paper a wet deposition scheme implemented in the GEOS-CHEM model and evaluate it against measurements of ^{210}Pb and ^{7}Be for specific meteorological years (1991–1994, 1996). Evaluations of

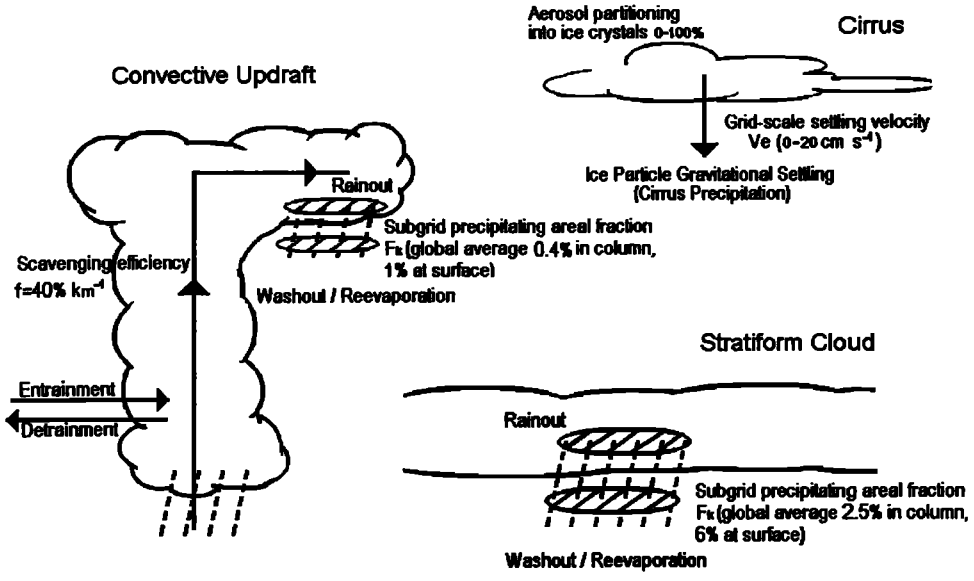

Figure 1. A schematic of moist transport and removal processes included in the model. These processes are aerosol scavenging within convective updrafts, first-order rainout and washout from convective anvils and stratiform precipitation, midlevel entrainment and detrainment, and cirrus precipitation. Some key parameters are identified: f is the scavenging efficiency of aerosol in a wet convective updraft (equation (1)), F_k is the fraction of the grid square area in vertical layer k that actually experiences precipitation, and V_e is the grid-scale settling velocity of cirrus ice particles (above 400 hPa). See text for details.

the GEOS precipitation fields and convective cloud tops have been presented by *Schubert et al.* [1993], *Molod et al.* [1996], and *Allen et al.* [1997]. Our simulation of moist transport and removal includes a new scheme for aerosol scavenging within convective updrafts, first-order rainout and washout from convective anvils and stratiform precipitation, midlevel convective entrainment and detrainment, and cirrus precipitation (Figure 1). The sensitivity of the simulation to these different processes in the context of reproducing the ^{210}Pb and ^{7}Be observations will be discussed. We will show some improvements over previous models in simulating latitudinal distributions and seasonal variations of ^{210}Pb and ^{7}Be. Consistency of meteorological fields between model and observations, as implemented here, improves the constraints for model evaluation. The latter consideration is particularly important for aircraft observations, which provide the only database of concentrations above the surface.

2. Model Description

2.1. General

The GEOS-CHEM model uses meteorological fields from the GEOS DAS available as a continuous archive with 3–6 hour resolution starting in 1985 [*Schubert et al.*, 1993]. The GEOS1 data for 1985–1994 have a resolution of 2° latitude by 2.5° longitude with 20 vertical sigma levels (top at 10 hPa). The midpoints of the lowest four levels are at ~ 50, 250, 600, and 1100 m above the surface. There are 14 levels below 150 hPa. The GEOS1-STRAT data for 1995–1997 have similar resolution in the troposphere but many additional layers in the stratosphere and a top at 0.1 hPa. We merged the upper 23 stratospheric levels in the GEOS1-STRAT (48–0.1 hPa) into 3 sigma levels. The simulations presented here use a degraded horizontal resolution (4° latitude × 5° longitude) for computational expediency. Sensitivity simulations were also conducted with the original 2° × 2.5° resolution. Degraded horizontal resolution has some consequence for the simulation of cross-tropopause transport, as discussed in section 2.6.

The model uses the advection scheme of *Lin and Rood* [1996], and the moist convective mixing scheme of *Allen et al.* [1996b] applied to the GEOS convective updraft, entrainment, and detrainment mass fluxes from the relaxed Arakawa-Schubert (RAS) algorithm [*Arakawa and Schubert*, 1974; *Moorthi and Suarez*, 1992]. We assume rapid vertical mixing within the GEOS-diagnosed mixed layer driven by surface instability [*Takacs et al.*, 1994]. The model is initialized for eight years, starting from low concentrations and recycling the meteorological fields for 1994, to equilibrate the lower stratosphere as well as the troposphere. We then conduct simulations through the period of 1990–1996 and analyze the specific years (1991–1994, 1996).

The GEOS data have been applied previously to simulations of ^{222}Rn [*Allen et al.*, 1996b], carbon monoxide (CO) [*Allen et al.*, 1996a] and dimethyl sulfide [*Chin et al.*, 1998]. The GEOS-CHEM model has been used more recently in several global investigations of tropospheric chemistry [*Bey et al.*, Global modeling of tropospheric chemistry with assimilated meteorology: Model description and evaluation, submitted to the *Journal of Geophysical Research*, 2001a, hereafter referred to as *Bey et al.*, submitted manuscript, 2001a; *Bey et al.*, Asian chemical outflow to the Pacific: Origins, pathways and budgets, submitted to the *Journal of Geophysical Research*, 2001b; *Li et al.*, 2000; *Palmer et al.*, 2001; *Singh et al.*, 2000].

2.2. Sources of ^{210}Pb and ^{7}Be

We assume a uniform ^{222}Rn emission of 1.0 atom cm^{-2} s^{-1} from land under nonfreezing conditions. Following *Jacob and Prather* [1990], we reduce the flux by a factor of 3 under freezing conditions. There is no emission from oceans or ice. Although observations show a large variability of ^{222}Rn emission from land, the above emission estimate is thought to be accurate to within 25% globally [*Turekian et al.*, 1977; B93] and to within a factor of 2 regionally [*Wilkening et al.*, 1975; *Schery et al.*, 1989; *Graustein and Turekian*, 1990; *Nazaroff*, 1992]. ^{222}Rn is an inert gas and its sole sink is radioactive decay to ^{210}Pb. Owing to its long half-life, almost all of the ^{210}Pb produced in the troposphere is removed by dry and wet deposition as opposed to radioactive decay.

Cosmic rays (mainly protons) penetrating into the Earth's atmosphere interact with atmospheric oxygen and nitrogen atoms to produce ^{7}Be [*Lal and Peters*, 1967, hereafter referred to as LP67]. Since cosmic particles tend to travel along the geomagnetic field, the ^{7}Be production rate is strongest over the poles. Maximum ^{7}Be production occurs in the stratosphere, reflecting the opposite vertical dependences of the cosmic ray flux and atmospheric density. About 2/3 of atmospheric ^{7}Be is generated in the stratosphere and 1/3 in the troposphere (LP67). The dependence of ^{7}Be production on season or longitude is negligible.

Published estimates of the ^{7}Be source distribution give global mean column production rates over an average solar cycle of 0.035 atoms cm^{-2} s^{-1} [*Masarik and Beer*, 1999], 0.063 atoms cm^{-2} s^{-1} [*O'Brien et al.*, 1991] and 0.081 atoms cm^{-2} s^{-1} (LP67), showing a large discrepancy. Following *Brost et al.* [1991] and K96, we use the LP67 source for 1958 (solar maximum year) because it yields the best simulation of stratospheric ^{7}Be concentrations measured from aircraft [*Leifer and Juzdan*, 1986; *Kritz et al.*, 1991; *Dibb et al.*, 1994]. In the stratosphere, ^{7}Be concentrations are determined by a balance between production and radioactive decay. In effect, we use the stratospheric ^{7}Be observations as a constraint on the ^{7}Be source.

The ^{7}Be production rate correlates inversely with solar activity [e.g., LP67; *Koch and Mann*, 1996]. At high solar activity, cosmic rays are deflected away from

the solar system and the ^{7}Be production rate is thus lower. The relative amplitude of the ^{7}Be production rate over a 11-year solar cycle ranges from 35% above 100 hPa in the polar regions, to 13% below 300 hPa at latitudes above 45°, to 4% in the lower atmosphere over the tropics (LP67). The effect on tropospheric ^{7}Be concentrations is relatively small and is ignored here; we assume no interannual variability in the ^{7}Be source. Shorter-term variations in the ^{7}Be source are negligible except for solar flares [LP67; *Brost et al.*, 1991]. Flare activity was relatively high in 1991 but very low during our other simulation years (1992–1994, 1996) (R. Thompson, personal communication, 2000).

2.3. Wet Deposition

Figure 1 gives a schematic of the ensemble of aerosol wet deposition processes included in the model. The GEOS model distinguishes between convective and stratiform precipitation. All water condensed under supersaturated conditions is immediately precipitated. Precipitation may reevaporate below cloud base. The hydrological data in the GEOS archive include 3-D fields of specific humidity change due to moist processes (Δq_m), but do not include partition between convective and stratiform precipitation fluxes except at the surface. Precipitation formation, evaporation, convective detrainment, and cumulus-induced subsidence all contribute to Δq_m [*Arakawa and Schubert*, 1974; *Moorthi and Suarez*, 1992]. We assume here that the contribution from the latter two processes is small, and further assume that Δq_m can be partitioned into convective and stratiform components on the basis of the precipitation flux data at the surface. Where there is no precipitation reaching the surface, precipitation in the column, if any, is assumed to be stratiform. These assumptions allow a full reconstruction of the 3-D convective and stratiform precipitation fields on the basis of the data in the GEOS archive.

There are some uncertainties involved in neglecting the contributions of liquid water detrainment and cumulus-induced subsidence to Δq_m [*Arakawa and Schubert*, 1974; *Moorthi and Suarez*, 1992]. Detrainment causes grid-scale moistening, while cumulus-induced subsidence causes grid-scale drying. Thus Δq_m overestimates the net condensation rate in most of the convective column and underestimates it near the top where large detrainment takes place.

2.3.1. Scavenging in convective updrafts. Following B93, we scavenge aerosols as part of the calculation of vertical transport in wet convective updrafts. Air lifted a distance dz in a wet updraft loses a fraction αdz of its aerosols, where α represents the scavenging efficiency. We assume that aerosols in the cloudy air are incorporated in the condensed phase of water, as is typically observed [*Jacob*, 2000]. The critical variables determining α are thus the conversion rate constant C_1 of cloud water to precipitation, for which we adopt $C_1 = 5 \times 10^{-3}$ s^{-1} [*Ogura and Takahashi*, 1971; *Ogura and Cho*, 1973; *Kain and Fritsch*, 1990; *Mari et al.*, 2001], and the updraft velocity w, for which we assume a typical continental value of 10 m s^{-1}. We obtain in this manner $\alpha = 5 \times 10^{-4}$ m^{-1}. For a convective column of thickness Δz, the fraction f of aerosol tracer scavenged by convective precipitation in the updraft is

$$f = 1 - e^{-\alpha \Delta z}. \quad (1)$$

In a 1-km deep updraft column 40% of the aerosol is scavenged. Thus, in a deep updraft the scavenging is complete, but in a shallow updraft a large fraction of the aerosol may escape scavenging. Updraft velocities in marine convection [*Jorgensen and LeMone*, 1989] are generally less than 10 m s^{-1}, but we find that the resulting increase in the scavenging efficiency has little effect on our simulation. Suppressing scavenging in shallow convective updrafts (tops shallower than 700 hPa), to account for less efficient precipitation formation, has less than a few percent effect anywhere.

2.3.2. Rainout and washout by stratiform and convective anvil precipitation. In addition to the scavenging in wet convective updrafts, we use the first-order rainout (in-cloud scavenging) parameterization of GC86 and the first-order washout (below-cloud scavenging) operator of B93 for both stratiform and convective precipitation. Rainout and washout from convective precipitation (not included in B93) are intended to represent precipitation from cloud anvils and are important for simulating the observed tropical ^{7}Be minimum, as discussed in section 5.

Rainout efficiently scavenges aerosols from a precipitating column. The critical variable is the fraction F_k of the grid square area in vertical layer k that actually experiences precipitation (B93). In GC86 this fraction is constrained by the grid-scale precipitation formation rate Q_k (kg m^{-3} s^{-1}), assuming constant values for the cloud condensed water content L (kg m^{-3}) and for the rate constant C_1 (s^{-1}) for conversion of cloud water to precipitation. For the top layer of a precipitating column we apply the formulations of GC86 for stratiform precipitation,

$$F_k = \frac{F_0 Q_k \Delta t}{L C_1 T_c} \quad (2)$$

and for convective precipitation,

$$F_k = \frac{F_0 Q_k \frac{\Delta t}{T_c}}{Q_k \frac{\Delta t}{T_c} + F_0 C_1 L} \quad (3)$$

where Δt is the model time step (30 min), T_c is the duration of precipitation over the time step (here $T_c = \Delta t$), and F_0 is a maximum value for F ($F_0 = 1$ for stratiform precipitation and $F_0 = 0.3$ for convective precipitation). For lower layers we further consider precipitation formation overhead to contribute to F_k, so that $F_k = \max(F_k, F_{k+1})$. This consideration is essential to the calculation of washout, described below.

Following GC86, we use $C_l = C_{l\,\min} + (Q_k/L)$ in (2), where $C_{l\,\min} = 1 \times 10^{-4}$ s^{-1} is a minimum value, and $C_l = 1.5 \times 10^{-3}$ s^{-1} in (3). For stratiform clouds we adopt $L = 1.5 \times 10^{-3}$ kg m^{-3}, as previously used by *Brost et al.* [1991] and *Rehfeld and Heimann* [1995]; using the original GC86 value $L = 0.5 \times 10^{-3}$ kg m^{-3} leads to too much scavenging in our model, as diagnosed by an underestimate of surface ^{210}Pb and ^{7}Be concentrations by ~ 15–20% on annual average. For convective clouds we use $L = 2.0 \times 10^{-3}$ kg m^{-3} as in GC86. We obtain in this manner global mean values $F_k = 2.5\%$ and $F_k = 0.4\%$ for 4° × 5° grid boxes experiencing stratiform and convective precipitation, respectively. The mean values at the surface, corresponding to the maximum values in the column overhead, are respectively $F_l = 6\%$ and $F_l = 1\%$. In our standard simulation we assume that rainout is suppressed at temperatures below 258 K because of the absence of riming, an assumption previously used by K96 and *Chin et al.* [1996]. The effect of this assumption will be examined in a sensitivity simulation.

Below-cloud washout by precipitation is calculated using a washout rate constant of 0.1 per mm of precipitation [*Dana and Hales*, 1976] applied to the precipitating fraction of the grid square (defined by the maximal value of F_k calculated in the cloudy column overhead). We also allow for release of scavenged aerosol during reevaporation of precipitation below cloud by carrying the scavenged aerosol load downward from level to level in the precipitating column. If a fraction f' of precipitation from overhead evaporates at a given vertical level, a corresponding fraction $0.5f'$ of the scavenged aerosol load is released at that level. The 0.5 factor is because some of the reevaporation of precipitation is by partial shrinking of the raindrops, which would not release aerosol. If $f' = 1$ (total reevaporation of precipitation), all of the scavenged aerosol load is released. Without this evaporative release, simulated aerosol concentrations in the lower troposphere would be 10% smaller at southern midlatitudes for ^{210}Pb and at southern/northern midlatitudes for ^{7}Be with less effect elsewhere.

2.4. Cirrus Precipitation

Lawrence and Crutzen [1998, hereafter referred to as LC98] pointed out that the gravitational settling of cloud particles may have an effect on HNO_3 concentrations in the upper troposphere and might also affect aerosols. The effect of this settling is to transport aerosols from the upper to the middle/lower troposphere. We apply the scheme only to cirrus precipitation, as defined by stratiform clouds above 400 hPa; we do not consider the gravitational settling of cloud liquid droplets, which generally have smaller settling velocities. A critical parameter for cirrus precipitation in LC98's scheme is the cloud ice water content (IWC), which is not available in the GEOS meteorological archive. We employ an empirical relationship from *Liou* [1986] between cirrus IWC (g m^{-3}) and temperature T (°C):

$$\ln(IWC) = -7.6 + 4e^{-0.2443\times10^{-3}(|T|-20)^{2.455}}, \quad |T| > 20°\text{C}. \tag{4}$$

The settling velocities of ice crystals are then computed following LC98 on the basis of the IWC and applied to the stratiform cloud fraction provided in the GEOS archive [*Takacs et al.*, 1994] to obtain grid-scale settling velocities V_e. Our calculated zonal mean values for V_e (typically 0–20 cm s^{-1}) are comparable to those in LC98.

The partitioning of aerosols into ice crystals in cirrus clouds is largely unknown. An observational case study indicates that ~ 40% of preexisting aerosol mass (16% of preexisting aerosol surface area) is incorporated in ice crystals [*Strom et al.*, 1997]. In order to bracket the range of cirrus precipitation effects we conduct simulations with either 0% and 100% partitioning of aerosols into ice crystals and adopt 100% as our standard case because of the better simulation it affords of ^{210}Pb and ^{7}Be observations in the middle and upper troposphere (see discussion in section 4).

2.5. Dry Deposition

Dry deposition of ^{210}Pb and ^{7}Be aerosols is computed using the resistance-in-series model of *Wesely and Hicks* [1977] as previously described by B93, K96, and *Chin et al.* [1996]. The calculated dry deposition velocities are 0.01–0.15 cm s^{-1} over oceans and 0.1–0.37 cm s^{-1} over land, reflecting differences in surface roughness height. The patterns and magnitudes are similar to those presented by *Chin et al.* [1996].

2.6. Adjustment of ^{7}Be Cross-Tropopause Flux

Stratosphere-troposphere exchange is crucial for simulation of ^{7}Be in the troposphere. The best constraint on the stratospheric contribution to tropospheric ^{7}Be comes from an analysis of the observed ^{7}Be/^{90}Sr ratio by *Dutkiewicz and Husain* [1985], showing that 23–27% of the ^{7}Be in surface air at northern midlatitudes is of stratospheric origin. To use this constraint, we separate stratospheric from tropospheric production of ^{7}Be in the model on the basis of the locally diagnosed thermal tropopause and simulate ^{7}Be produced in the stratosphere as a separate tracer. Results indicate excessive cross-tropopause transport in the GEOS archive, which we can choose to correct artificially by scaling down the stratospheric ^{7}Be source in the simulation of tropospheric ^{7}Be. The reduction required is a factor of 4 in the GEOS1 archive with 4° × 5° horizontal resolution, a factor of 3 in the same archive with 2° × 2.5° resolution, and a factor of 3.5 in the GEOS1-STRAT archive with 4° × 5° resolution. These scaling factors are adopted in our standard simulation for simulating tropospheric

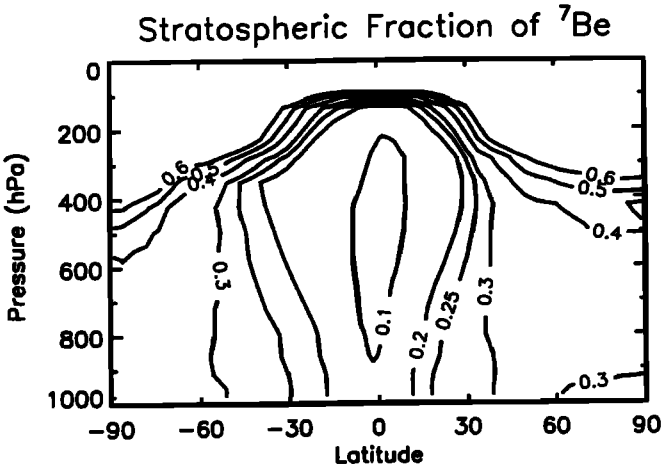

Figure 2. Stratospheric fraction of zonal mean tropospheric ^{7}Be concentrations in the standard model simulation for 1994 as a function of latitude and pressure. Values are annual averages from the GEOS1 simulation with 4° × 5° resolution. The ^{7}Be source in the stratosphere (diagnosed from the local model tropopause) has been reduced by a factor of 4 to correct for excessive cross-tropopause transport in the model.

^{7}Be (Figure 2); they are not used for simulating stratospheric ^{7}Be. The impact of cross-tropopause transport on tropospheric ^{210}Pb is insignificant. As shown in section 3.2, simulation of ^{7}Be deposition fluxes provides further support for scaling down the cross-tropopause transport in the model.

The excessive cross-tropopause transport of ^{7}Be identified in the present study is consistent with the tropospheric ozone simulation of *Bey et al.* (submitted manuscript, 2001a) with the GEOS-CHEM model, which indicates a factor of 3–4 overestimate of the cross-tropopause flux of ozone in the GEOS1 archive with 4° × 5° resolution. Bey et al. (submitted manuscript, 2001a) found that although the magnitude of the cross-tropopause ozone flux is too large, the latitudinal and seasonal variations of that flux are consistent with current knowledge. This result suggests that a uniform reduction in the cross-tropopause transport of ^{7}Be, as implemented here, should not induce large errors in the latitudinal or seasonal distribution of this transport.

3. Simulation Results for 1994 and Evaluation With Surface Data

3.1. Budgets and Global Distributions

Table 1 gives the annual average global budgets of ^{210}Pb and ^{7}Be in the model troposphere for 1994. The tropopause is determined in the model using a criterion of 2 °C km^{-1} lapse rate as defined by the World Meteorological Organization (WMO). Wet deposition is the dominant sink. The tropospheric residence time of ^{210}Pb is 9 days, which is at the high end of the 5–9 days range from previous studies [*Turekian et al.*, 1977; B93; K96; *Guelle et al.*, 1998b; *Giannakopoulos et al.*, 1999; *Rasch et al.*, 2000]. Radioactive decay accounts for 19% of the ^{7}Be sink in the troposphere, less than K96 (29%) but much higher than *Brost et al.* [1991] where it is negligibly small. The tropospheric residence time of ^{7}Be against deposition is 21 days, consistent with K96 (21 days) and the 22–35 days range from *Bleichrodt* [1978] obtained by comparing observed air concentrations with deposition fluxes at 30-75°N.

Figure 3 shows zonal mean, annual average concentrations of ^{210}Pb and ^{7}Be for 1994 in the standard simulation (Figures 3a and 3b) and in the simulation with no scavenging of aerosol by cirrus precipitation (Figures 3c and 3d). Concentrations are expressed in mixing ratio units of millibequerels per standard cubic meter (at 0°C and 1 atm pressure) or mBq SCM^{-1}. The ^{210}Pb concentration in the model lower stratosphere is 0.1–0.2 mBq SCM^{-1} in both hemispheres. Observations indicate stratospheric ^{210}Pb concentrations of 0.2–0.4 mBq SCM^{-1} [*Feely and Seitz*, 1970; *Environmental Measurements Laboratory*, 2000a]. The model underestimate of ^{210}Pb in the stratosphere is one drawback brought by the inclusion of aerosol scavenging by cirrus precipitation. Without cirrus precipitation, the model gives about 0.4 mBq SCM^{-1} in the Northern Hemisphere (NH) and ~ 0.3 mBq SCM^{-1} in the Southern Hemisphere (SH), closer to the observations (Figure 3c).

The model simulates a minimum ^{210}Pb concentration in the tropical upper troposphere, as was also found in the model of *Giannakopoulos et al.* [1999], and is due to efficient scavenging of ^{210}Pb in deep convective updrafts. Cirrus precipitation also contributes to this minimum in our model, as seen by comparing Figures 3a and 3c. The ^{7}Be concentrations show a minimum in the tropical upper troposphere in the standard simulation but not in that with cirrus precipitation suppressed (Figures 3b and 3d). Tropospheric ^{7}Be concentrations

Table 1. Annual Average Global Budgets of ^{210}Pb and ^{7}Be in the Model Troposphere for 1994

	^{210}Pb	^{7}Be
Burden, g	299	2.7
Residence time, days	9	21[a]
Sources, g d^{-1}	34	0.16
from stratosphere	—	0.03
within troposphere	34	0.13
Sinks, g d^{-1}	34	0.16
dry deposition	3.8	0.01
wet deposition		
stratiform	9.6	0.04
convective	21	0.08
radioactive decay	0.03	0.03

[a]Against deposition only. The actual residence time including loss from radioactive decay is 17 days. The tropopause is determined in the model using a criterion of 2 °C km^{-1} lapse rate as defined by World Meteorological Organization.

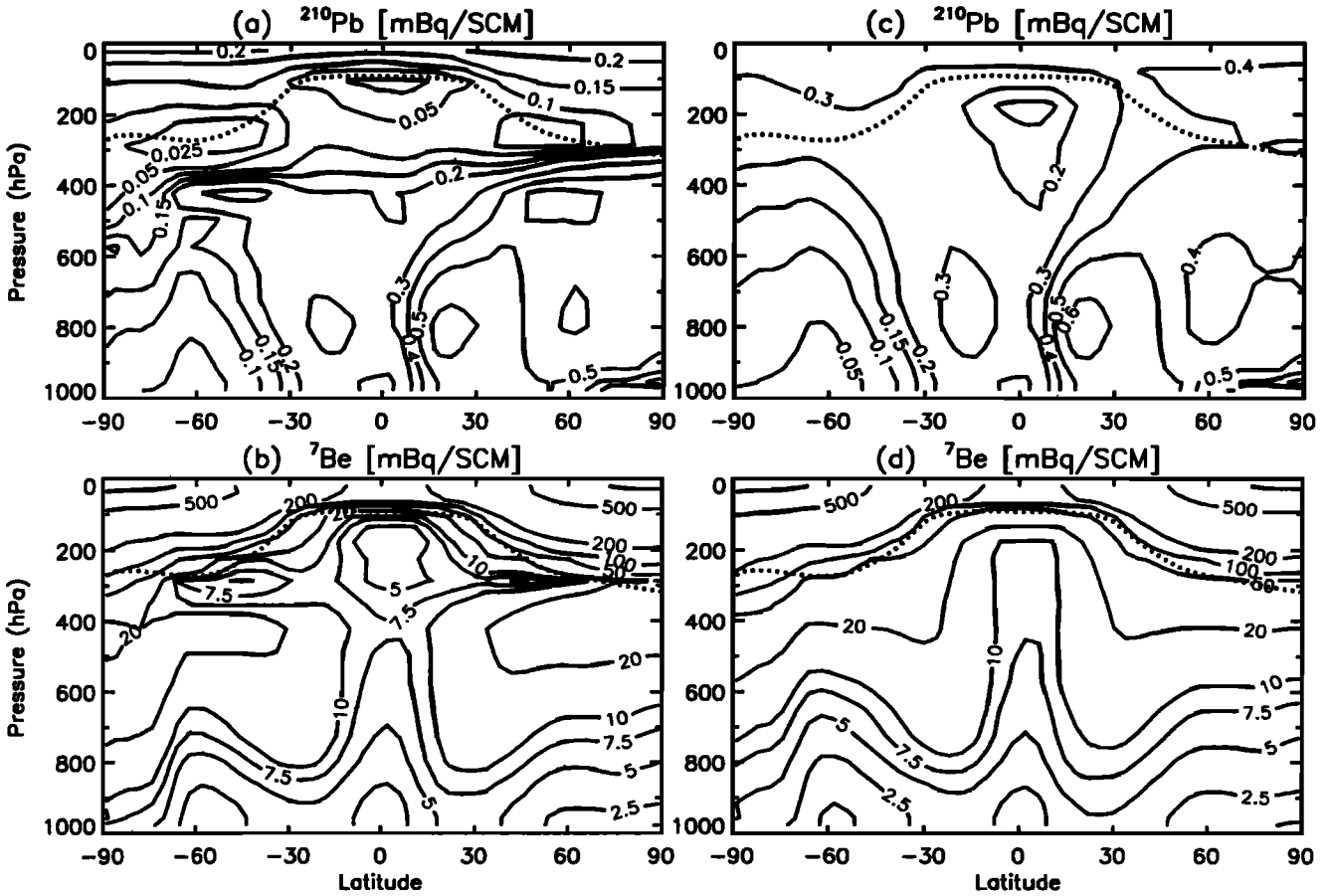

Figure 3. Zonal mean mixing ratios (mBq SCM^{-1}) of (a) ^{210}Pb and (b) ^{7}Be in the standard simulation as a function of latitude and pressure. (c, d) Same as Figures 3a and 3b, except that aerosol scavenging by cirrus precipitation is excluded. Values are annual averages for 1994. For the simulation of ^{7}Be in the troposphere the ^{7}Be source in the stratosphere (diagnosed from the local model tropopause) has been reduced by a factor of 4 to correct for excessive cross-tropopause transport in the model (section 2.6); this reduction is not applied to the simulation of ^{7}Be in the stratosphere. The dotted line is the annual average tropopause height.

are maximum in the dry descending branches of the Hadley circulation over the subtropics, as well as over Antarctica. As mentioned in section 2.2, the ^{7}Be concentration in the model stratosphere is consistent with aircraft measurements.

Figure 4 shows the simulated global distributions of monthly mean ^{210}Pb concentrations for January and July 1994, at the surface and at 500 hPa, in the standard simulation. The highest ^{210}Pb concentrations in surface air are over arid continental regions. The model captures the high aerosol concentrations in the Arctic lower troposphere in winter caused by long-range boundary layer transport of Eurasian air over the Arctic and then North America with little precipitation along its trajectory [*Barrie*, 1986]. Another large-scale pattern well simulated by the model is the Asian monsoon circulation, which causes ^{210}Pb concentrations in surface air over eastern Asia to be much higher in winter than in summer. Simulated ^{210}Pb concentrations in the free troposphere (500 hPa) are generally higher in summer than in winter due to stronger convective activity.

Similar plots for ^{7}Be are shown in Figure 5. The highest concentrations are in the dry subsiding subtropics and over high plateaus (Antarctica, Greenland, Tibet). Strong seasonal variation in ^{7}Be is found over southern Asia because of the monsoons. Lowest ^{7}Be concentrations in surface air are found in the SH midlatitudes owing to scavenging by frequent large-scale precipitation. The intertropical convergence zone (ITCZ), which is characterized by strong convergence and convective precipitation, is also associated with low ^{7}Be concentrations. The overall patterns of horizontal distribution and seasonal variation at the surface are similar to those reported by *Rehfeld and Heimann* [1995].

3.2. Deposition Fluxes

We compare in Figure 6 the model-simulated annual mean total deposition fluxes of ^{210}Pb and ^{7}Be for 1994

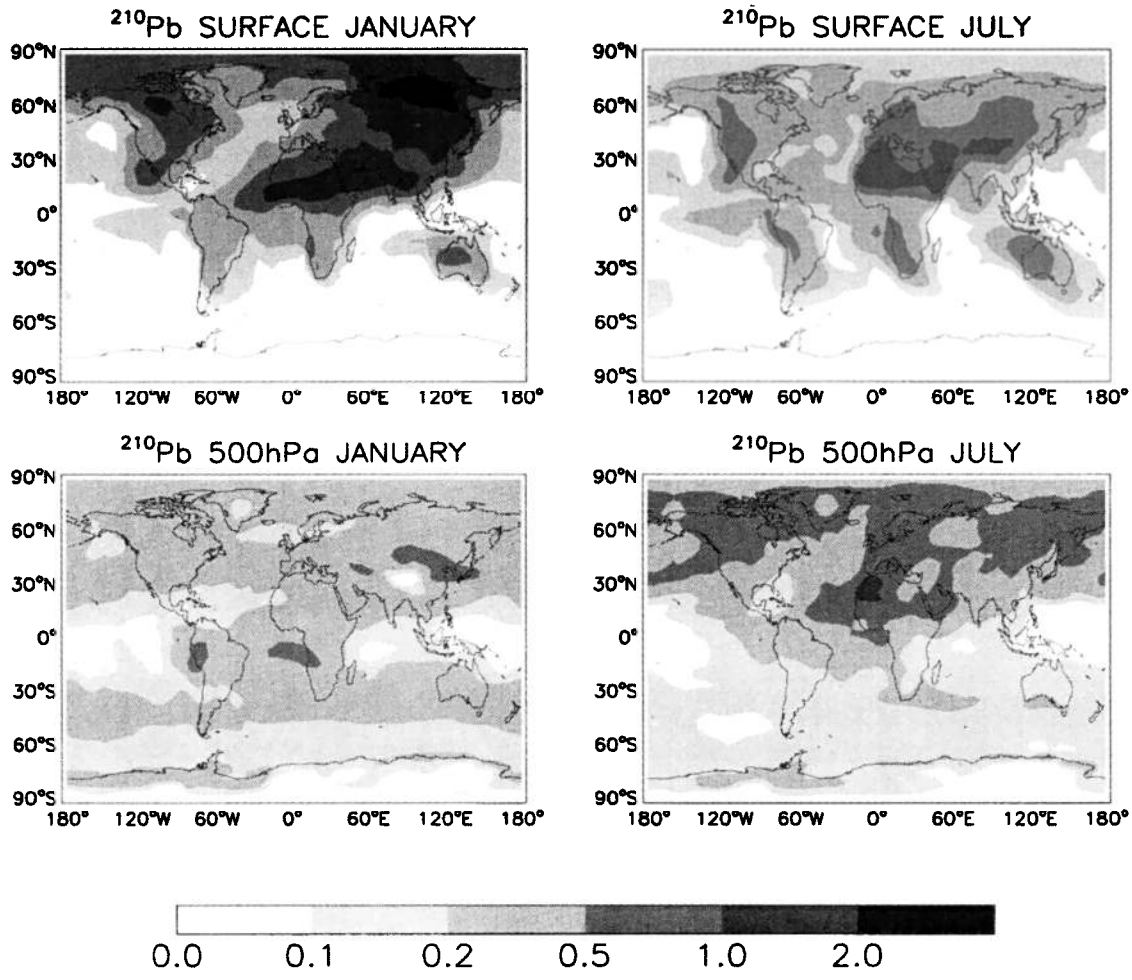

Figure 4. Simulated global distributions of monthly mean ^{210}Pb concentrations (mBq SCM^{-1}) for January and July 1994 at the surface and at 500 hPa. The darkest shading denotes values greater than 2.0 mBq SCM^{-1}.

at 63 (^{210}Pb) and 25 (^{7}Be, northern midlatitude) sites from which long-term records of observations are available. The ^{210}Pb deposition flux observations are from the compilation of *Feichter et al.* [1991] and the ^{7}Be deposition flux observations are from the compilation of K96. The model captures well the magnitude and latitudinal distribution of both ^{210}Pb and ^{7}Be deposition fluxes. We define the mean model bias γ as in K96:

$$\gamma = \frac{\sum_j ([x]_{\text{model},j} - [x]_{\text{observation},j})}{\sum_j [x]_{\text{observation},j}}, \qquad (5)$$

where x is either ^{210}Pb or ^{7}Be, and the sum is over all measurement sites j. $\gamma = 0$ means no mean bias. The overall model biases are -13% for ^{210}Pb and 11% for ^{7}Be. The bias for ^{210}Pb is largely due to high observed concentrations at three Japan sites (Hachijojima, Kanazawa, and Nagasaki), which have been attributed previously to anomalously high ^{222}Rn emission from eastern Asia [*Jacob et al.*, 1997]. Without these three sites the model bias for ^{210}Pb would be -2%. The relatively small bias in the simulation of the ^{7}Be deposition flux reflects the factor of 4 scaling of the cross-tropopause flux in the model (section 2.6). Without this scaling, the model bias for ^{7}Be would be 108% (Figure 6). The ^{7}Be deposition flux thus offers a sensitive test of the simulation of cross-tropopause transport in global models.

3.3. Surface Air Concentrations

Climatological records of ^{210}Pb and ^{7}Be concentrations in surface air are available from sites around the globe and can be used to evaluate our model. We used the data sets compiled by K96. Figure 7 compares the simulated and observed annual average concentrations of ^{7}Be at 88 sites and ^{210}Pb at 44 sites as a function of latitude. Model results are for 1994. The model overestimates ^{7}Be concentrations at three mountain sites (Tenerife, Mauna Loa, and Chacaltaya), shown as symbols in Figure 7; the model at these sites samples the free troposphere, but the observations may frequently

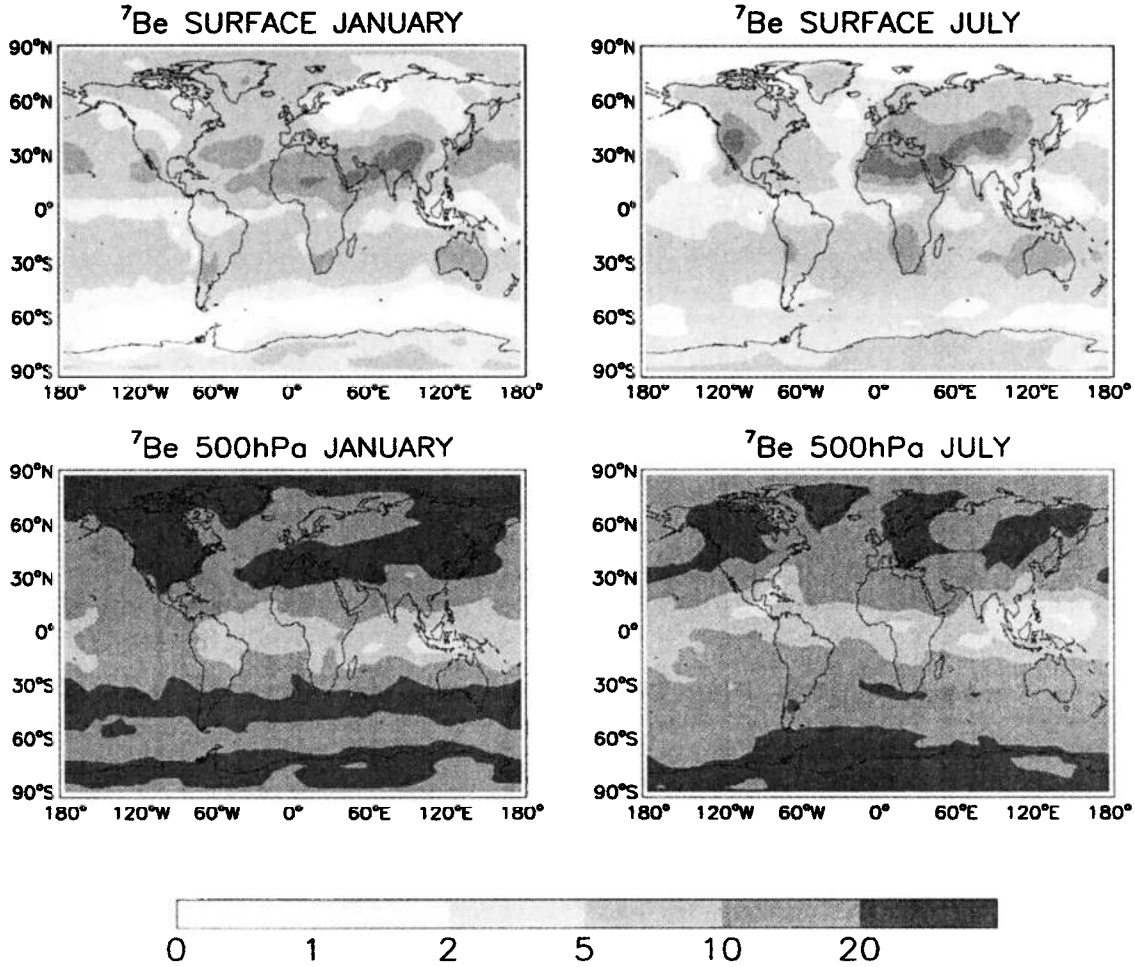

Figure 5. Same as Figure 4, except for ^{7}Be concentration (mBq SCM^{-1}). The darkest shading denotes values greater than 20 mBq SCM^{-1}.

sample boundary layer air in upslope flow and depositional effects would also be more important than the corresponding altitude sampled by the model. Excluding these three sites, the mean model biases are 17% for ^{7}Be and 1% for ^{210}Pb. Latitudinal trends are well simulated. The model captures the observed ^{7}Be maxima in the subtropics and over Antarctica associated with subsidence. It also captures the observed concentration minimum of ^{7}Be in the tropics, which has been a difficulty for earlier models. This minimum results from rapid scavenging within the ITCZ, and its simulation in the model is contingent on the accounting of rainout in convective anvils, as discussed in section 5. The low ^{7}Be concentrations observed at midlatitudes are well simulated and are due to efficient scavenging in the midlatitude storm tracks.

Simulated seasonal variations of ^{210}Pb and ^{7}Be concentrations are compared in Figure 8 with 1991–1994 measurements at seven representative locations [*Larsen et al.*, 1995; *Environmental Measurements Laboratory*, 2000b]. We did not use the same year for all locations because of limitations on data availability. However, the model and observed fields are always for the same meteorological years. Also plotted as dots are the climatological means defined by the multiyear observational record.

Thule is an arctic station, with high concentrations of both ^{210}Pb and ^{7}Be in winter and low concentrations in summer. The model reproduces this seasonal variation. Without suppression of in-cloud scavenging below 258 K the wintertime simulation is slightly degraded (dot-dashed line in Figure 8). Other arctic sites show the same seasonal pattern, both in the observations and in the model.

Rexburg (elevation 1502 m) is a high-plateau continental site located in the western central United States. The observed ^{210}Pb concentration shows a strong seasonal variation with minimum in summer and maximum in winter, while the observed ^{7}Be shows the opposite phase, consistent with the seasonal variation of convective mixing at midlatitudes [*Feely et al.*, 1989]. Other continental midlatitude sites show similar seasonal variations in the observations. The model captures well the seasonal phase for ^{7}Be, but underestimates ^{210}Pb in

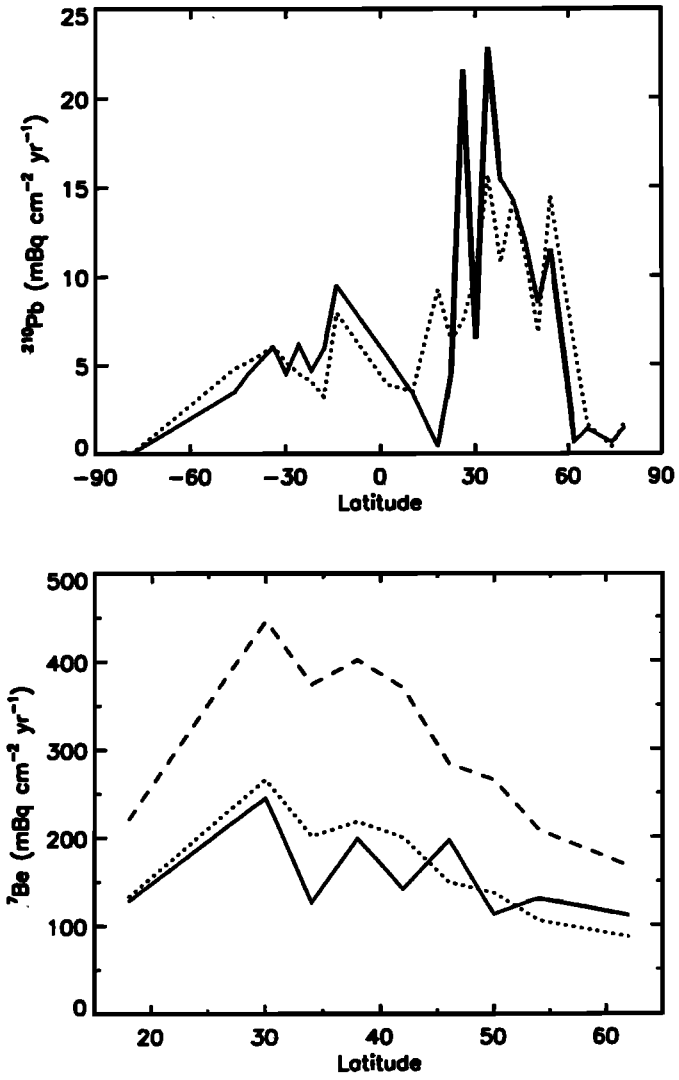

Figure 6. Observed (solid line) and simulated (dotted line) annual average total deposition fluxes of ^{210}Pb (at 66 sites) and ^{7}Be (at 25 sites) as a function of latitude. The data from individual sites are averaged over 4° latitudinal bins. The observations are for the ensemble of years available [*Feichter et al.*, 1991; K96]. The ^{7}Be sites are all in the 19-60°N latitudinal band. Model results are for 1994. The dashed line for ^{7}Be shows results from the simulation without adjustment of the cross-tropopause flux (section 2.6).

winter and overestimates ^{7}Be in summer. The former problem was previously encountered by B93 and *Lee and Feichter* [1995], who attributed it to wintertime stratification not resolved by the model. Uncertainty in estimating ^{222}Rn emission from frozen soil may also contribute. The overestimate of ^{7}Be in summer may reflect the difficulty previously described in simulating high-altitude surface stations.

Miami in the United States is a subtropical coastal station. The ^{7}Be concentrations are highest in winter-spring, reflecting the seasonal variation of local precipitation [*Feely et al.*, 1989]. The model is in close agreement with observations for the same meteorological year. Simulated ^{210}Pb concentrations are much lower than observed, as also found in a previous model study [*Lee and Feichter*, 1995], and possibly reflecting the coastal nature of the site. ^{210}Pb concentrations sampled in an adjacent continental grid box in the model are much closer to the observations.

The seasonal variation of ^{210}Pb concentrations at Guayaquil, Ecuador (a tropical site), shows a maximum in austral winter, both in the 1992 observations and in the model, resulting from the seasonal variation in precipitation. The seasonal variation of ^{7}Be is weak, both in the observations and in the model.

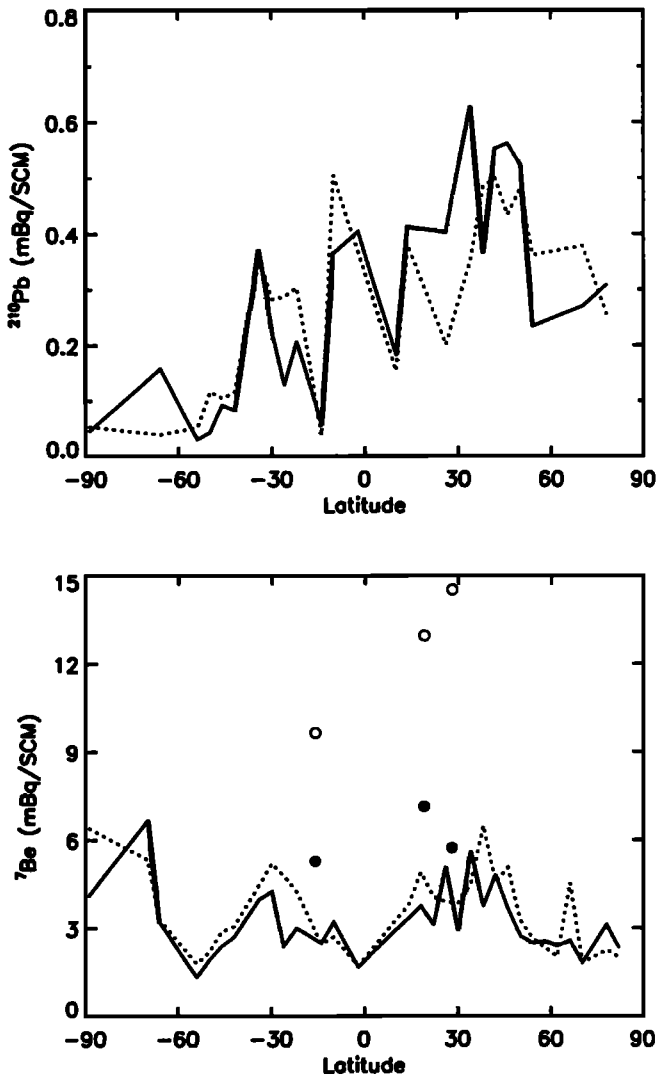

Figure 7. Observed (solid line) and simulated (dotted line) annual average surface concentrations of ^{210}Pb (47 sites) and ^{7}Be (91 sites) as a function of latitude. The data from individual sites are averaged over 4° latitudinal bins. The observations are for the ensemble of years available (K96). Model results are for 1994. Symbols show the observed (dots) and model (circles) annual average ^{7}Be surface concentrations at three mountain sites (Tenerife, Mauna Loa, and Chacaltaya).

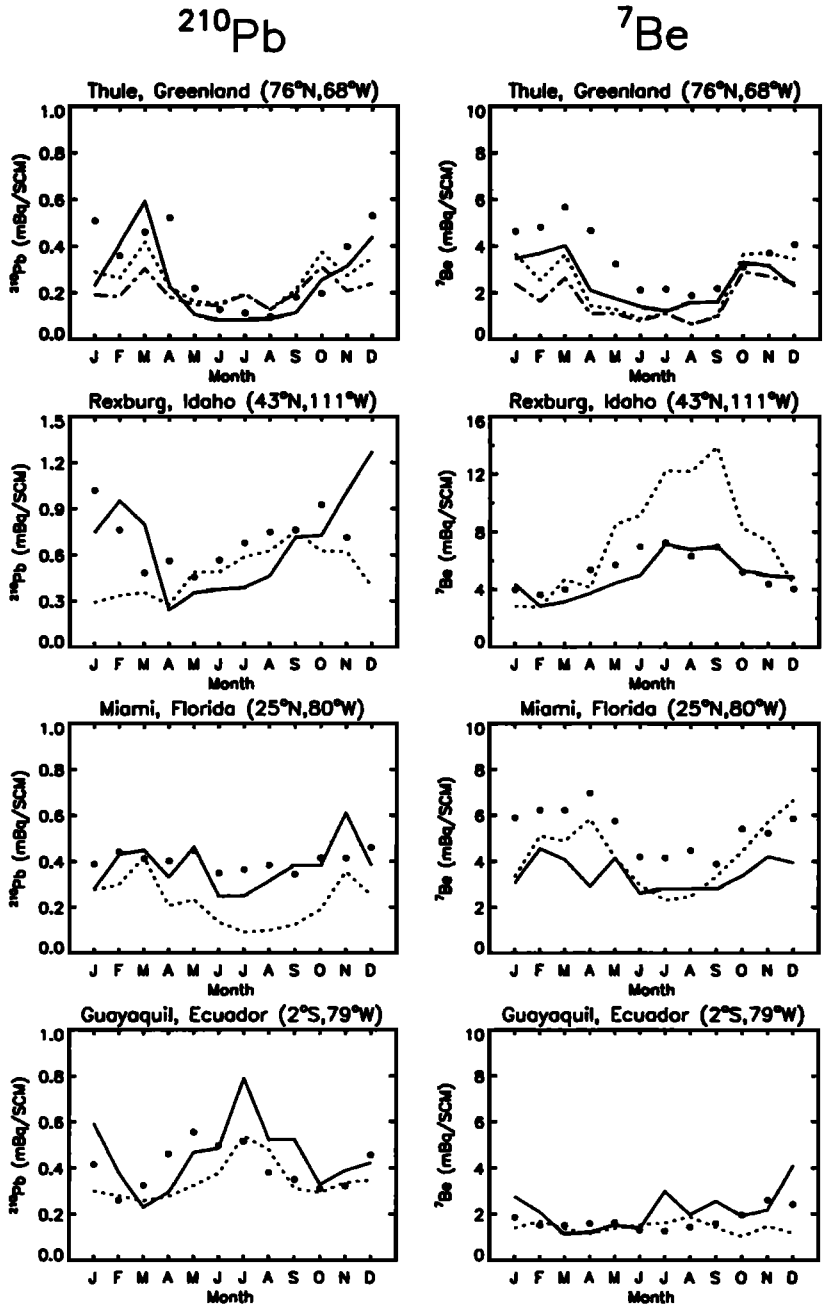

Figure 8. Comparison between observed (solid line) and simulated (dotted line) seasonal variations of ^{210}Pb and ^{7}Be concentrations at the sites of Thule (1994), Rexburg (1993), Miami (1991), Guayaquil (1992), Tutuila (1994), Santiago (1992), and South Pole Station (1991). The model simulation uses meteorological data for the appropriate year. Also shown as dots are the long-term climatologies of observations at the sites for ^{210}Pb (K96) and ^{7}Be [*Feely et al.*, 1989]. The dot-dashed lines for Thule and South Pole Station indicate the model results for a simulation where in-cloud scavenging below 258 K is not suppressed (the effect at other sites is negligibly small).

Observed and modeled ^{210}Pb concentrations at American Samoa are low due to the remoteness from continents. The June-October maximum in both ^{210}Pb and ^{7}Be observations is well captured in the model and corresponds to the dry season of the southern tropics, when aerosol scavenging is less frequent than during the rest of the year. The model of *Giannakopoulos et al.* [1999] underestimated the ^{210}Pb concentrations at this station but did show the elevated spring ^{210}Pb. *Feely et al.* [1989] previously attributed to precipitation most of the seasonal variation in the ^{7}Be observations at Samoa. Another contributing factor would be the subsidence of southern midlatitude air, which is most frequent in winter [*Harris and Oltmans*, 1997].

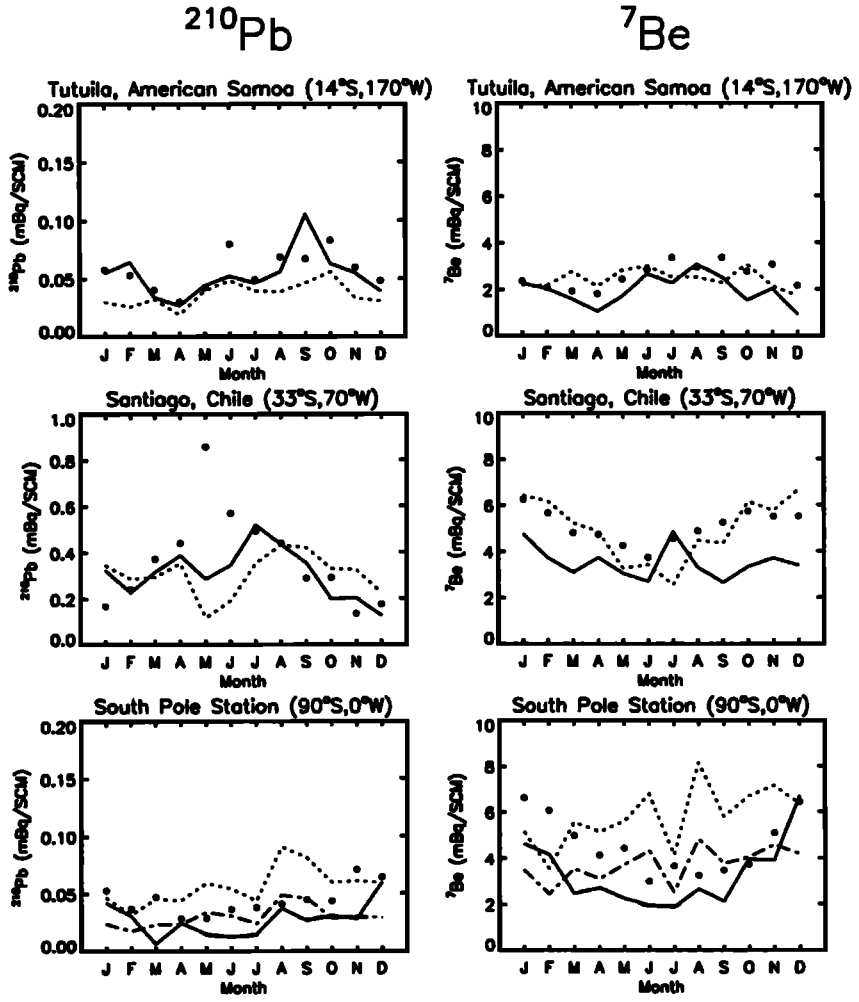

Figure 8. (continued)

Santiago, Chile, is a subtropical coastal site. The observed concentrations of ^{210}Pb are maximum in winter and minimum in summer; for ^{7}Be the seasonal variation is reversed. These opposite trends are consistent with the greater intensity of convective vertical mixing in summer than in winter. The model reproduces the observed seasonal variation of ^{7}Be but shows no simple seasonal variation for ^{210}Pb. There is a May-June minimum in the simulated ^{210}Pb concentrations that exaggerates a similar feature seen in the 1992 observations (though not in the climatology). This May-June minimum in the model is due to anomalously high precipitation.

Observed ^{210}Pb and ^{7}Be concentrations at South Pole Station are maximum in summer and minimum in winter, presumably reflecting the seasonal variation of subsidence. The model captures neither magnitude nor seasonal phase for both tracers. We find that without cirrus precipitation the model would reproduce the observed seasonal variation of ^{7}Be although the amplitude is less. Simulation of ^{210}Pb over Antarctica has been a consistent difficulty in atmospheric models [*Rasch et al.*, 2000]. Without suppression of in-cloud scavenging below 258 K the simulation of magnitude for both ^{210}Pb and ^{7}Be is improved (dot-dashed line in Figure 8).

4. Vertical Profiles

Surface sites offer only limited constraints on the simulation of ^{210}Pb and ^{7}Be. In this section we present a comparison of model results with observations up to 12-km altitude from two aircraft missions, PEM-West B over the Northwest Pacific (February-March 1994) [*Dibb et al.*, 1997] and PEM-Tropics A over the South Pacific (September-October 1996) [*Dibb et al.*, 1999a, 1999b]. The PEM-West B and PEM-Tropics A data sets contain 140 and 280 ^{210}Pb and ^{7}Be aerosol samples, respectively. Sample integration time was 20–30 min. In PEM-West B all ^{210}Pb samples are above the detection limit (0.02 mBq SCM^{-1}), and 84% of the ^{7}Be samples are above the detection limit (0.56 mBq SCM^{-1}). In PEM-Tropics A all ^{210}Pb samples are above the detection limit (3.7×10^{-3} mBq SCM^{-1}), and 69% of the ^{7}Be samples are above the detection limit (3.7 mBq SCM^{-1}). A value equal to half of the detection limit is assumed for those ^{7}Be samples below the detection

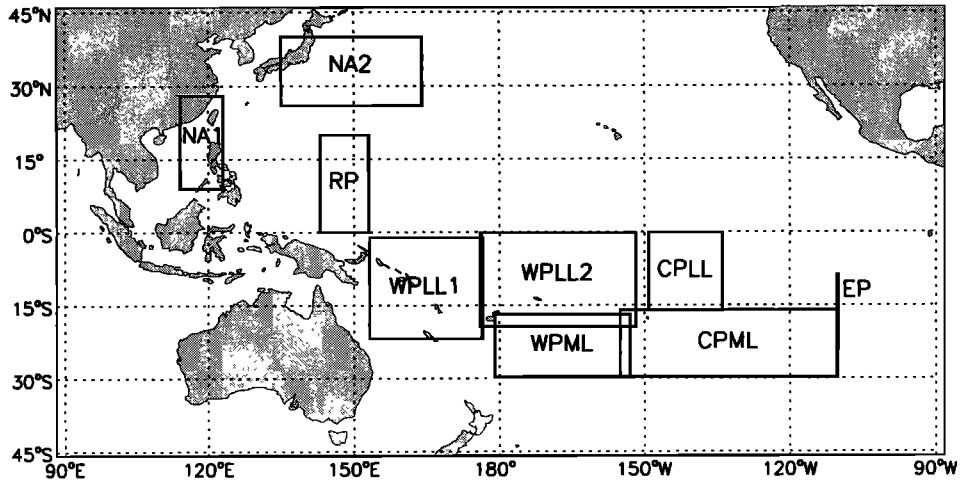

Figure 9. Selected regions for comparison of model results with aircraft observations for ^{210}Pb and ^{7}Be from PEM-West B and PEM-Tropics A. The choice of regions is that of *Dibb et al.* [1997] for PEM-West B and that of *Fenn et al.* [1999] for PEM-Tropics A. The PEM-West B regions are remote Pacific (RP) and near Asia (NA1 and NA2); the PEM-Tropics A regions are western Pacific low latitude (WPLL1 and WPLL2), western Pacific middle latitude (WPML), central Pacific low latitude (CPLL), central Pacific middle latitude (CPML), and eastern Pacific (EP).

limit. The model is sampled within each region over the time period of the measurements, using the GEOS meteorological archives for the appropriate years (1994 and 1996).

4.1. PEM-West B

We compare simulated and observed vertical distributions of ^{210}Pb and ^{7}Be concentrations over three regions (Figure 9) where intensive flights were flown. Following *Dibb et al.* [1997] we call these regions "remote Pacific" (RP) and "near Asia" (NA1 and NA2). The comparisons are shown in Figure 10. The ^{210}Pb observations indicate a generally decreasing trend with altitude, particularly over the NA regions which were most affected by Asian outflow. Strong Asian outflow over the western Pacific during PEM-West B was largely confined to the lower troposphere [*Merrill et al.*, 1997]. The Asian outflow in the model is shifted upward relative to observations, with low ^{210}Pb concentrations simulated in the marine boundary layer.

In the RP region, concentrations of ^{7}Be in the middle troposphere are overestimated in the model. This overestimate is not of stratospheric origin, as determined in a simulation with the stratospheric ^{7}Be source shut off (dot-dot-dashed lines in Figure 10). Examination of the GEOS1 and GEOS1-STRAT archives indicates that there is very little precipitation formation (and hence aerosol rainout) in the middle troposphere (3–9 km) north of the equator, particularly in the RP region. Furthermore, there is evidence that wet convective transport in the GEOS1 connects the PBL and the upper troposphere too directly, underestimating entrainment and hence aerosol scavenging in the middle troposphere [*Schubert and Rood*, 1995].

We find that cirrus precipitation is important for the simulation of ^{210}Pb and ^{7}Be in the middle and upper troposphere for the RP and NA1 regions. Without cirrus precipitation the model yields higher concentrations than observed (long dashes in Figure 10). For NA2 the inclusion of cirrus precipitation degrades the simulation at the highest altitudes, which are however in the stratosphere. As we will see, cirrus precipitation also improves simulation of high-altitude observations during PEM-Tropics A.

4.2. PEM-Tropics A

In Figure 11 we compare model and aircraft measurements for six regions sampled in PEM-Tropics A (Figure 9): central Pacific lower latitude (CPLL), central Pacific midlatitude (CPML), eastern Pacific (EP), western Pacific midlatitude (WPML), and western Pacific low latitude (WPLL1 and WPLL2). *Fenn et al.* [1999] used a similar grouping in their study of air mass characterization during PEM-Tropics A. A major feature of observations in that mission was the frequent encounter in the free troposphere of continental layers, a few kilometers thick, with high levels of biomass burning pollution [*Fuelberg et al.*, 1999]. These layers were mainly associated with fast westerly transport of subsiding air originating from over southern Africa and South America, although there also were some instances of easterly transport of layers from South America to the equatorial eastern Pacific [*Blake et al.*, 1999]. The layers are apparent as high ^{210}Pb observations in Figure 11 although the long averaging time of the ^{210}Pb measurement precludes resolution of the layer structure. High ^{7}Be concentrations were often observed in the layers, presumably reflecting the subsidence.

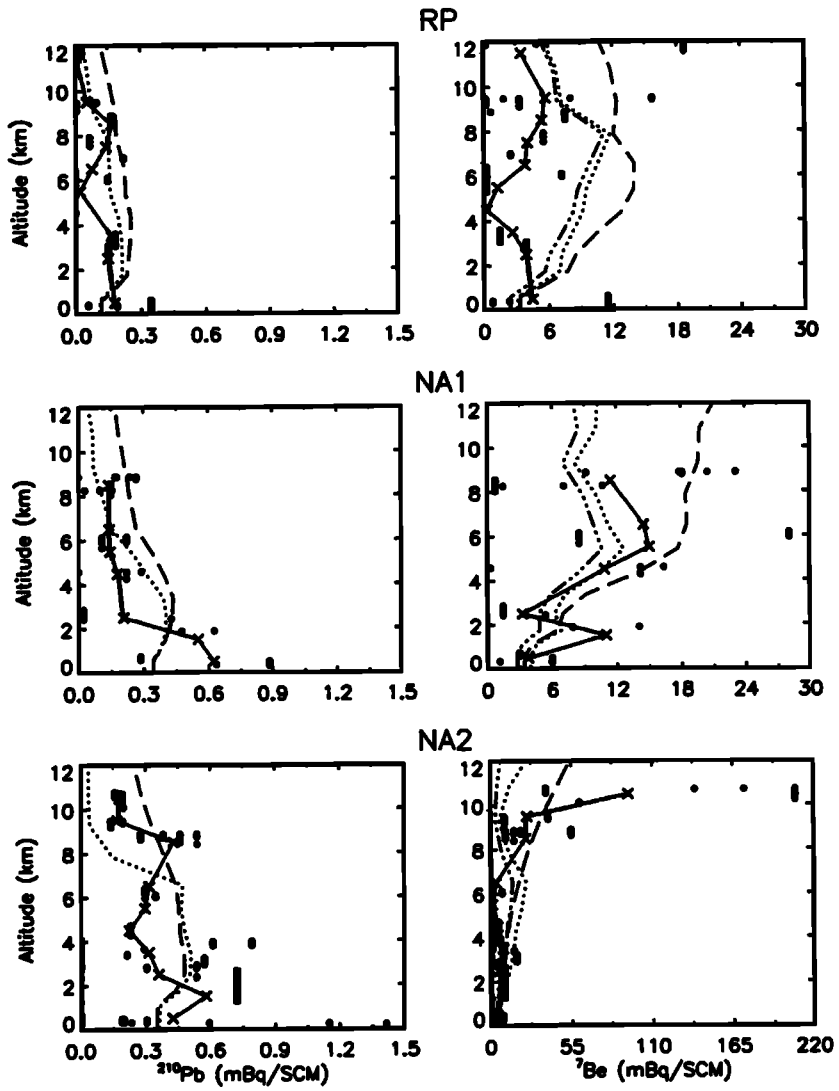

Figure 10. Comparison between simulated (dotted line) and observed (solid line) vertical distributions of (left) ^{210}Pb and (right) ^{7}Be during PEM-West B for the three regions of Figure 9: remote Pacific (RP) and near Asia (NA1 and NA2). Dot-dot-dashed lines show model results for a simulation where the stratospheric ^{7}Be source is shut off. Long-dashed lines show model results for a simulation where aerosol scavenging by cirrus precipitation (section 2.4) is excluded. Individual aircraft measurements are shown as dots and the corresponding 1-km averages are shown as crosses. Note the larger scale for ^{7}Be at NA2. See text for details.

The model captures qualitatively the observed middle troposphere ^{210}Pb enhancements associated with continental layers in PEM-Tropics A, particularly in the WPML region where they were most frequently encountered. The ^{210}Pb enhancements in the model are accompanied by slight ^{7}Be enhancements, reflecting subsidence during the long-range transport of continental air over the Pacific. The simulated ^{210}Pb peak in the lower troposphere in the EP region matches the easterly outflow from South America observed in PEM-Tropics A [*Blake et al.*, 1999]; no ^{210}Pb measurements were made in that outflow. The observations of ^{7}Be in PEM-Tropics A show considerable variability, which may reflect the self-induced stability of dry layers subsiding from the upper troposphere [*Stoller et al.*, 1999]. The model does not capture this variability but falls within the envelope of the observations. Stratospheric influence is small over all the regions (Figure 11).

The sensitivity simulation without cirrus precipitation shows large overestimates for ^{210}Pb in almost all regions and for ^{7}Be in the CPML and WPML regions. Again, these results lend some support for cirrus precipitation representing a significant downward transport mechanism for aerosols.

Allen et al. [1997] evaluated deep convective mixing in the GEOS1 archive and concluded that, although the location of deep convective mixing in the tropics is reasonably well simulated, the frequency is overestimated in the tropics. However, this overestimate is not apparently seen in our simulations of ^{210}Pb and ^{7}Be. Simulated profiles of ^{210}Pb and ^{7}Be in the tropics (e.g., regions of RP, CPLL, EP, WPLL1, and WPLL2) show

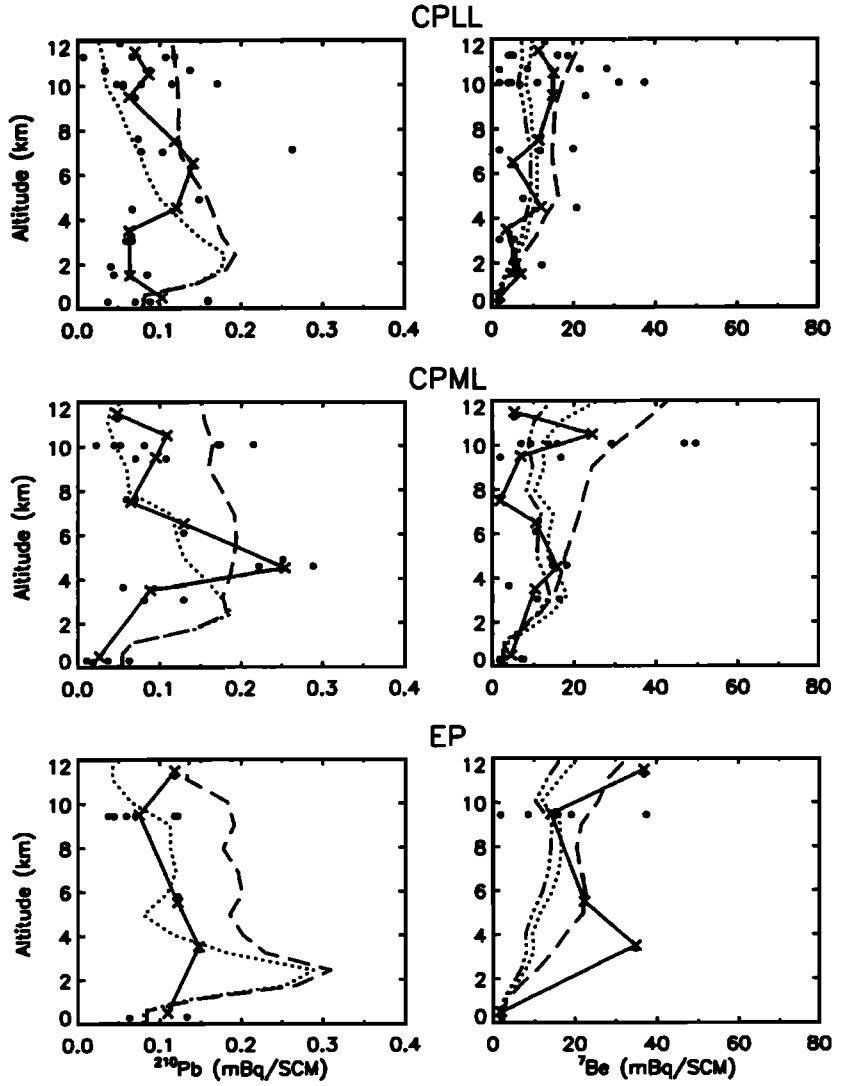

Figure 11. Comparison between simulated (dotted line) and observed (solid line) vertical distribution of (left) ^{210}Pb and (right) ^{7}Be during PEM-Tropics A over the six regions of Figure 9: western Pacific low latitude (WPLL1 and WPLL2), western Pacific middle latitude (WPML), central Pacific low latitude (CPLL), central Pacific middle latitude (CPML), and eastern Pacific (EP). Dot-dot-dashed lines are for a simulation where stratospheric ^{7}Be source is shut off. Long-dashed lines are for a simulation where cirrus precipitation (section 2.4) is excluded. Individual aircraft measurements are shown as dots and the corresponding 1-km averages are shown as crosses. See text for details.

vertical gradients between 3 km and 10 km that are generally similar to the observed, except for ^{7}Be in RP, WPLL1, and WPLL2. For the region of RP it is a different problem (section 4.1). For WPLL1 and WPLL2, although the simulated ^{7}Be profiles has relatively small vertical gradient in the middle and upper troposphere, it is difficult to be conclusive because the ^{7}Be observations show considerable variability as well as thin layers.

5. Sensitivity Studies

Simulation of aerosol scavenging in global models, where precipitation is subgrid in scale and the mechanisms for precipitation formation are crudely parameterized, involves a number of assumptions. In this section we discuss how our simulation of ^{210}Pb and ^{7}Be improves constraints on these assumptions.

The lack of significant global bias in our simulations of ^{210}Pb and ^{7}Be concentrations and deposition fluxes at surface sites lends some confidence in our scheme for modeling the scavenging of aerosols on a global scale. It gives support to our model estimates of the global mean tropospheric residence times of ^{210}Pb and ^{7}Be against deposition, 9 and 21 days, respectively.

We conducted sensitivity simulations to test different aspects of our wet deposition schemes. In the scheme for scavenging in convective updrafts, an important parameter is the conversion rate constant C_1 from cloud water to precipitation, for which we used a typical value of 5×10^{-3} s^{-1} recommended by *Mari et al.* [2000].

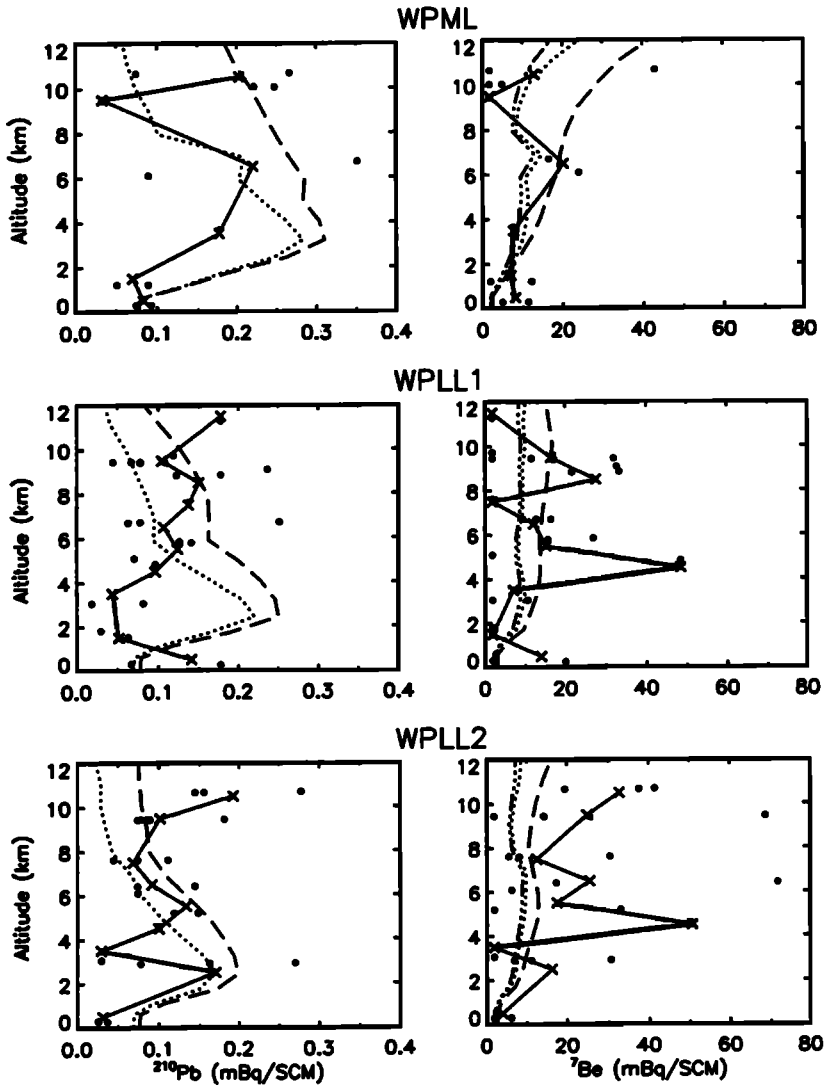

Figure 11. (continued)

Values of C_1 in the literature range from 1.5×10^{-3} s^{-1} (GC86) to 10^{-2} s^{-1} [*Kain and Fritsch*, 1990], which imply scavenging efficiencies (i.e., f in equation (1)) in the range 14–63% per km of updraft (section 2.3.1). We find that using a scavenging efficiency of 14% km^{-1} increases ^{210}Pb concentrations by ~10% in most of the troposphere and up to 27% in the tropical upper troposphere, and increases ^{7}Be concentrations by up to 18% in the lower troposphere in the tropics and southern midlatitudes, compared with the standard simulation (40% km^{-1}). Such increases would degrade simulations of the observed surface air concentrations for both ^{210}Pb and ^{7}Be (section 3.3). Using 63% km^{-1} decreases concentrations by less than 10% anywhere relative to the standard simulation.

One improvement on previous models is the simulation of the tropical minimum in surface ^{7}Be concentrations. We found in sensitivity tests that the inclusion of first-order rainout loss in convective precipitation, allowing for scavenging by anvils outside the updraft, is primarily responsible for this success; without it the ^{7}Be concentrations in the tropics and subtropics would be significantly overestimated. Lead 210 is not as sensitive as ^{7}Be to this scavenging process, again stressing the necessity of using both ^{7}Be and ^{210}Pb to test algorithms for wet scavenging. Our results suggest an important role for anvil precipitation in aerosol scavenging in the tropics. Anvil precipitation is mainly caused by the horizontal transport of condensate from convective updrafts and it can account for half or more of the total precipitation in tropical regions [*Cheng and Houze*, 1979; *Gamache and Houze*, 1983; *Tiedtke*, 1993].

We stated in section 2.3.2 that rainout from stratiform clouds is sensitive to the specification of the cloud condensed water content, for which we used 1.5×10^{-3} kg m^{-3} [*Brost et al.*, 1991; *Rehfeld and Heimann*, 1995]. Using 0.5×10^{-3} kg m^{-3} as in GC86 decreases tropospheric ^{210}Pb and ^{7}Be concentrations by 10–40% at middle and high latitudes, significantly degrading the simulation. For rainout by stratiform and convective

precipitation we assumed that no scavenging occurs below 258 K due to absence of riming [K96; *Chin et al.*, 1996]. Without this suppression of in cloud scavenging, the annual average tropospheric concentrations in polar regions would be reduced by 15–40% (^{210}Pb) and 15–30% (^{7}Be). Polar observations do not offer a clear diagnostic of which assumption is better (section 3.3). Finally, we find that below-cloud scavenging (washout) is only a minor sink for ^{210}Pb or ^{7}Be. Without washout the simulated concentrations throughout the troposphere would change by less than 10%.

Simulating cirrus precipitation with the gravitational settling scheme for cloud ice particles proposed by LC98 greatly improves the simulations of ^{210}Pb and ^{7}Be in the free troposphere (Figures 10 and 11). Aerosol scavenging by rainout, as diagnosed in the GEOS archive, is relatively inefficient in the upper and middle troposphere. Cirrus precipitation compensates for this inefficiency. Excluding cirrus precipitation in the model would imply less stratospheric influence on ^{7}Be at the surface and would therefore require a smaller reduction factor in the GEOS cross-tropopause transport to meet the *Dutkiewicz and Husain* [1985] constraint (section 2.6). The reduction factor would be 3 in the GEOS1 archive with 4° × 5° horizontal resolution, as compared to 4 in the standard simulation. Using this smaller reduction factor, the model biases in a sensitivity simulation without aerosol scavenging by cirrus precipitation are −11% (^{210}Pb) and -3% (^{7}Be) for the total deposition flux observations (Figure 6), and 1% (^{210}Pb) and −4% (^{7}Be) for surface air concentrations in 1994 (Figure 7). Simulation of the surface air concentrations is thus slightly improved when cirrus precipitation is suppressed. The corresponding tropospheric residence times of ^{210}Pb and ^{7}Be are 11 and 30 days, respectively.

6. Summary and Conclusions

In this paper we have tested the ability of a global 3-D model driven by the GEOS assimilated meteorological data to simulate ^{210}Pb and ^{7}Be, two natural aerosol tracers originating from different source regions (lower troposphere and upper troposphere/lower stratosphere, respectively) and removed from the troposphere principally by wet deposition. Our simulation of moist transport and removal includes scavenging in convective updrafts with a scavenging efficiency of 40% km^{-1}, midlevel convective entrainment and detrainment, first-order rainout/washout from both convective anvils and stratiform precipitation, and cirrus precipitation. To test the wet deposition scheme, we have compared the model simulation results of both ^{210}Pb and ^{7}Be aerosols with surface observations for 1991–1994 and vertical profiles from two large-scale aircraft missions over the Pacific (PEM-West B and PEM-Tropics A).

Observations of the ^{7}Be deposition flux and of the ^{7}Be/^{90}Sr concentration ratio in surface air offer sensitive tests of cross-tropopause transport in global models. Results indicate excessive cross-tropopause transport in the GEOS meteorological data. The reduction required to match the observations are a factor of 4 in the GEOS1 data with 4° × 5° horizontal resolution, a factor of 3 in the same archive with 2° × 2.5° resolution, and a factor of 3.5 in the GEOS1-STRAT archive with 4° × 5° resolution.

With this correction to the cross-tropopause flux the model provides a good simulation of ^{210}Pb and ^{7}Be surface concentrations and deposition fluxes; it shows some success in reproducing the observed latitudinal and seasonal distributions, often improving on previous models. One particular improvement is the simulation of the tropical ^{7}Be minimum, enabled by inclusion of a first-order rainout loss associated with convective precipitation. This result suggests that convective cloud anvil precipitation may be an important mechanism for aerosol scavenging in the tropics. Global mean tropospheric lifetimes of ^{210}Pb and ^{7}Be against deposition in the model are 9 and 21 days, respectively.

Simulation of vertical profiles (0–12 km altitude) measured from aircraft is highly sensitive to the inclusion of aerosol scavenging by cirrus precipitation in the model, although we cannot exclude the possibility that cirrus precipitation is in fact covering up for insufficient precipitation formation at high altitudes in the GEOS archive. Without cirrus precipitation, observed concentrations in the middle and upper troposphere would be greatly overestimated. The effect of cirrus precipitation on concentrations in the lower troposphere is small. Our understanding of aerosol partitioning in cirrus clouds is still lacking, and simulation of these clouds in global models is a challenge. Further work is needed to better assess the role of cirrus precipitation as a mechanism for aerosol removal from the upper troposphere.

The model captures the frequent long-range transport of continental air masses observed over the South Pacific during PEM-Tropics A, although it does not resolve the layered vertical structure of the observations. The continental layers sampled in PEM-Tropics A followed subsiding trajectories originating from the upper troposphere over the tropical continents, where deep convection connected the continental boundary layer to the upper troposphere and supplied in particular ^{222}Rn. This mechanism may explain the presence of both elevated ^{210}Pb and ^{7}Be in the continental layers over the South Pacific, in the observations as well as in the model.

Sensitivity studies were conducted to test the constraints offered by observations on the different components of our wet deposition schemes. Decreasing the scavenging efficiency in wet convective updrafts to much less than 40% km^{-1} would degrade simulations of the surface air observations for both ^{210}Pb and ^{7}Be. Increasing the scavenging efficiency in convective updrafts has little effect since scavenging is nearly complete in any case. Suppression of scavenging in shallow wet convection is also found to have little effect. Rainout from

convective anvils (outside the updrafts) is critical for simulation of the observed ^{7}Be tropical minimum. The rainout rate constant for stratiform clouds is also an important parameter. Below-cloud scavenging (washout) and reevaporation (virga) have little effect.

Simulation of ^{7}Be together with ^{210}Pb in a model driven by assimilated meteorological fields has provided a valuable constraint for improving the representation of precipitation scavenging of aerosols in the model and has also helped to identify the strong and weak aspects of the model. Vertical profiles measured from aircraft through the tropospheric column are of particular value and more of these measurements are needed. Inclusion of ^{210}Pb and ^{7}Be measurements in aircraft campaigns investigating convective transport and scavenging processes would be extremely profitable. Finally, efforts to reduce the uncertainties in the estimate of ^{7}Be source strength should be encouraged.

Acknowledgments. We are very grateful to Dorothy Koch who helped us with the ^{210}Pb and ^{7}Be data sets. We wish to thank Mian Chin, Paul DeMott, Brian Toon, and Cindy Twohy for useful discussions, Jozef Masarik for his ^{7}Be source data and Andrea Molod for information on the GEOS archive. Suggestions given by Jennifer Logan and anonymous reviewers were helpful. ^{210}Pb and ^{7}Be data for 1991–1994 are provided by the Environmental Measurements Laboratory (EML) through its Web site (http://www.eml.doe.gov/). This work was funded by the National Aeronautics and Space Administration.

References

Allen, D. J., P. Kasibhatla, A. M. Thompson, R. B. Rood, B. G. Doddridge, K. E. Pickering, R. D. Hudson, and S.-J. Lin, Transport-induced interannual variability of carbon monoxide determined using a chemistry and transport model, *J. Geophys. Res.*, *101*, 28,655-28,669, 1996a.

Allen, D. J., R. B. Rood, A. M. Thompson, and R. D. Hudson, Three-dimensional radon 222 calculations using assimilated meteorological data and a convective mixing algorithm, *J. Geophys. Res.*, *101*, 6871–6881, 1996b.

Allen, D. J., K. E. Pickering, and A. Molod, An evaluation of deep convective mixing in the Goddard Chemical Transport Model using International Satellite Cloud Climatology Project cloud parameters, *J. Geophys. Res.*, *102*, 25,467–25,476, 1997.

Arakawa, A., and W. H. Schubert, Interaction of cumulus cloud ensemble with the large-scale environment, Part I, *J. Atmos. Sci.*, *31*, 671–701, 1974.

Balkanski, Y.J., D.J. Jacob, G.M. Gardner, W.C. Graustein, and K.K. Turekian, Transport and residence times of tropospheric aerosols inferred from a global three-dimensional simulation of ^{210}Pb, *J. Geophys. Res.*, *98*, 20,573–20,586, 1993.

Barrie, L. A., Arctic air pollution: An overview of current knowledge, *Atmos. Environ.*, *20*, 643–663, 1986.

Blake, N. J., et al., Influence of southern hemispheric biomass burning on midtropospheric distributions of nonmethane hydrocarbons and selected halocarbons over the remote South Pacific, *J. Geophys. Res.*, *104*, 16,213–16,232, 1999.

Bleichrodt, J.F., Mean tropospheric residence time of cosmic -ray-produced beryllium 7 at north temperate latitudes, *J. Geophys. Res.*, *83*, 3058–3062, 1978.

Bondietti, E. A., C. Papastefanou, and C. Rangarajan, Aerodynamic size associations of natural radioactivity with ambient aerosols, in *Radon and Its Decay Products: Occurrence, Properties and Health Effects, Symp. Ser. 331*, edited by P. K. Hopke, pp. 377–397, Am. Chem. Soc., Washington, D. C., 1987.

Bondietti, E. A., J. N. Brantley, and C. Rangarajan, Size distributions and growth of natural and Chernobyl-derived submicron aerosols in Tennessee, *J. Environ. Radioact.*, *6*, 99–120, 1988.

Brost, R.A., J. Feichter, and M. Heimann, Three-dimensional simulation of ^{7}Be in a global climate model, *J. Geophys. Res.*, *96*, 22,423–22,445, 1991.

Cheng, C.-P., and R. A. Houze Jr., The distribution of convective and mesoscale precipitation in GATE radar echo patterns, *Mon. Weather Rev.*, *107*, 1370–1381, 1979.

Chin, M., D. J. Jacob, G. M. Gardner, M. S. Foreman-Fowler, and P. A. Spiro, A global three-dimensional model of tropospheric sulfate, *J. Geophys. Res.*, *101*, 18,667–18,690, 1996.

Chin, M., R. B. Rood, D. J. Allen, M. O. Andreae, A. M. Thompson, S.-J. Lin, R. M. Atlas, and J. V. Ardizzone, Processes controlling dimethylsulfide over the ocean: Case studies using a 3-D model driven by assimilated meteorological fields, *J. Geophys. Res.*, *103*, 8341–8353, 1998.

Dana, M. T., and J. M. Hales, Statistical aspects of the washout of polydisperse aerosols, *Atmos. Environ.*, *10*, 45–50, 1976.

Dibb, J. E., R. W. Talbot, and G. L. Gregory, ^{7}Be and ^{210}Pb in the western hemisphere arctic atmosphere: Observations from the three recent aircraft-based sampling programs, *J. Geophys. Res.*, *97*, 16,709–16,715, 1992.

Dibb, J. E., L. D. Meeker, R. C. Finkel, J. R. Southon, M. W. Caffee, and L. A. Barrie, Estimation of stratospheric input to the Arctic troposphere: ^{7}Be and ^{10}Be in aerosols at Alert, Canada, *J. Geophys. Res.*, *99*, 12,855–12,864, 1994.

Dibb, J. E., R. W. Talbot, B. L. Lefer, E. Scheuer, G. L. Gregory, E. V. Browell, J. D. Bradshaw, S. T. Sandholm, and H. B. Singh, Distribution of beryllium 7 and lead 210, and soluble aerosol-associated ionic species over the western Pacific: PEM West B, February - March 1994, *J. Geophys. Res.*, *102*, 28,287-028,302, 1997.

Dibb, J. E., R. W. Talbot, L. D. Meeker, E. M. Scheuer, N. J. Blake, D. R. Blake, G. L. Gregory and G. W. Sachse, Constraints on the age and dilution of Pacific Exploratory Mission-Tropics biomass burning plumes from the natural radionuclide tracer ^{210}Pb, *J. Geophys. Res.*, *104*, 16,233–16,241, 1999a.

Dibb, J. E., R. W. Talbot, E. M. Scheuer, D. R. Blake, N. J. Blake, G. L. Gregory, G. W. Sachse, and D. C. Thornton, Aerosol chemical composition and distribution during the Pacific Exploratory Mission (PEM) Tropics, *J. Geophys. Res.*, *104*, 5785–5800, 1999b.

Dutkiewicz, V. A., and L. Husain, Stratospheric and tropospheric components of ^{7}Be in surface air, *J. Geophys. Res.*, *90*, 5783–5788, 1985.

Environmental Measurements Laboratory, High Altitude Sampling Program Database, http:// www.eml.doe.gov/, Dep. of Energy, New York, 2000a.

Environmental Measurements Laboratory, Surface Air Sampling Program Database, http:// www.eml.doe.gov/, Dep. of Energy, New York, 2000b.

Feely, H. W., and H. Seitz, Use of lead 210 as a tracer of transport processes in the stratosphere, *J. Geophys. Res.*, *75*, 2885–2894, 1970.

Feely, H. W., R. J. Larsen, and C. G. Sanderson, Factors that cause seasonal variations in beryllium-7 concentra-

tions in surface air, *J. Environ. Radioactivity, 9*, 223–249, 1989.

Feichter, J., R.A. Brost, and M. Heimann, Three-dimensional modeling of the concentration and deposition of ^{210}Pb aerosols, *J. Geophys. Res., 96*, 22,447–22,460, 1991.

Fenn, M. A., et al., Ozone and aerosol distributions and air mass characteristics over the South Pacific during the burning season, *J. Geophys. Res., 104*, 16,197–16,212, 1999.

Fuelberg, H. E., R. E. Newell, S. P. Longmore, Y. Zhu, D. J. Westberg, E. V. Browell, D. R. Blake, G. L. Gregory, and G. W. Sachse, A meteorological overview of the Pacific Exploratory Mission (PEM) Tropics period, *J. Geophys. Res., 104*, 5585–5622, 1999.

Gamache, J. F., and R. A. Houze, Water budget of a mesoscale convective system in the tropics, *J. Atmos. Sci., 40*, 1835–1850, 1983.

Giannakopoulos, C., M. P. Chipperfield, K. S. Law, and J. A. Pyle, Validation and intercomparison of wet and dry deposition schemes using ^{210}Pb in a global three-dimensional off-line chemical transport model, *J. Geophys. Res., 104*, 23,761–23,784, 1999.

Giorgi, F., and W. L. Chameides, Rainout lifetimes of highly soluble aerosols and gases as inferred from simulations with a general circulation model, *J. Geophys. Res., 91*, 14,367–14,376, 1986.

Graustein, W. C., and K. K. Turekian, Radon fluxes from soils to the atmosphere measured by ^{210}Pb-^{226}Ra disequilibrium in soils, *Geophys. Res. Lett., 17*, 841–844, 1990.

Guelle, W., Y. J. Balkanski, J. E. Dibb, M. Schulz, and F. Dulac, Wet deposition in a global size-dependent aerosol transport model, 2, Influence of the scavenging scheme on ^{210}Pb vertical profiles, surface concentrations, and deposition, *J. Geophys. Res., 103*, 28,875–28,891, 1998a.

Guelle, W., Y. J. Balkanski, M. Schulz, F. Dulac, and P. Monfray, Wet deposition in a global size-dependent aerosol transport model, 1, Comparison of a 1 year ^{210}Pb simulation with ground measurement, *J. Geophys. Res., 103*, 11,429–11,445, 1998b.

Harris, J. M., and S. J. Oltmans, Variations in tropospheric ozone related to transport at American Samoa, *J. Geophys. Res., 102*, 8781–8791, 1997.

Intergovernmental Panel on Climate Change, *IPCC third assessment report (TAR) expert review*, World Meteorol. Org., Geneva, Switzerland, 2000.

Jacob, D. J., Heterogeneous chemistry and tropospheric ozone, *Atmos. Environ., 34*, 2131-2159, 2000.

Jacob, D. J., and M. J. Prather, Radon-222 as a test of boundary layer convection in a general circulation model, *Tellus, Ser. B, 42*, 118–134, 1990.

Jacob, D. J., et al., Evaluation and intercomparison of global atmospheric transport models using ^{222}Rn and other short-lived tracers, *J. Geophys. Res., 102*, 5953–5970, 1997.

Jorgensen, D. P., and M. A. LeMone, Vertical velocity characteristics of oceanic convection, *J. Atmos. Sci., 46*, 621–640, 1989.

Kain, J. S., and J. M. Fritsch, A one-dimensional entraining detraining plume model and its application in convective parameterization, *J. Atmos. Sci., 47*, 2784–2802, 1990.

Kasibhatla, P. S., H. Levy II, W. J. Moxim, and W. L. Chameides, The relative impact of stratospheric photochemical production on tropospheric NO_y levels: A model study, *J. Geophys. Res., 96*, 18,631–18,646, 1991.

Kiehl, J. T., T. L. Schneider, P. J. Rasch, M. C. Barth, and J. Wong, Radiative forcing due to sulfate aerosols from simulations with the National Center for Atmospheric Research Community Climate Model, Version 3, *J. Geophys. Res., 105*, 1441–1457, 2000.

Koch, D. M., and M. E. Mann, Spatial and temporal variability of ^{7}Be surface concentrations, *Tellus, Ser. B, 48*, 387–396, 1996.

Koch, D. M., D. J. Jacob, and W. C. Graustein, Vertical transport of tropospheric aerosols as indicated by ^{7}Be and ^{210}Pb in a chemical tracer model, *J. Geophys. Res., 101*, 18,651–18,666, 1996.

Koch, D. M., D. J. Jacob, I. Tegen, D. Rind, and M. Chin, Tropospheric sulfur simulation and sulfate direct radiative forcing in the Goddard Institute for Space Studies general circulation model, *J. Geophys. Res., 104*, 23,799–23,822, 1999.

Kritz, M. A., S. W. Rosner, E. F. Danielsen, and H. B. Selkirk, Air mass origins and troposphere-to-stratosphere exchange associated with midlatitude cyclogenesis and tropopause folding inferred from ^{7}Be measurements, *J. Geophys. Res., 96*, 17,405–17,414, 1991.

Lal, D., and B. Peters, Cosmic ray produced radioactivity on the Earth, in *Handbuch der Physik*, 46/2, edited by K. Sitte, pp. 551–612, Springer-Verlag, New York, 1967.

Lal, D., P. K. Malhotra, and B. Peters, On the production of radioisotopes in the atmosphere by cosmic radiation and their application to meteorology, *J. Atmos. Terr. Phys., 12*, 306–328, 1958.

Lambert, G., B. Ardouin, and J. Sanak, Atmospheric transport of trace elements toward Antarctica, *Tellus, Ser. B, 42*, 76–82, 1990.

Larsen, R. J., C. G. Sanderson, and J. Kada, EML Surface Air Sampling Program 1990–1993 data, USDOE Rep. EML-572, U.S. Dep. of Energy, Washington, D. C., Nov. 1995.

Lawrence, M. G., and P. J. Crutzen, The impact of cloud particle gravitational settling on soluble trace gas distributions, *Tellus, Ser. B, 50*, 263–289, 1998.

Lee, H. N., and J. Feichter, An intercomparison of wet precipitation scavenging schemes and the emission rates of ^{222}Rn for the simulation of global transport and deposition of ^{210}Pb, *J. Geophys. Res., 100*, 23,253–23,270, 1995.

Leifer, R., and Z. R. Juzdan, The high altitude sampling program: Radioactivity in the stratosphere, final report, December 1986, *EML-Rep.-458*, Environ. Meas. Lab., Dep. of Energy, New York, 1986.

Li, Q., D. J. Jacob, I. Bey, R. M. Yantosca, Y. Zhao, and Y. Kondo, Atmospheric hydrogen cyanide (HCN): Biomass burning source, ocean sink?, *Geophys. Res. Lett., 27*, 357–360, 2000.

Lin, S.-J., and R. B. Rood, Multidimensional flux-form semi-Lagrangian transport schemes, *Mon. Weather Rev., 124*, 2046–2070, 1996.

Liou, K.-N., Influence of cirrus clouds on weather and climate processes: A global perspective, *Mon. Weather Rev., 114*, 1167–1199, 1986.

Maenhaut, W., W. H. Zoller, and D. G. Coles, Radionuclides in the South Pole atmosphere, *J. Geophys. Res., 84*, 3131–3138, 1979.

Mari, C., D. J. Jacob, and P. Bechtold, Transport and scavenging of soluble gases in a deep convective cloud, *J. Geophys. Res., 105*, 22,255–22,267, 2000.

Masarik, J., and J. Beer, Simulation of particle fluxes and cosmogenic nuclide production in the Earth's atmosphere, *J. Geophys. Res., 104*, 12,099–12,111, 1999.

Merrill, J. T., Atmospheric long-range transport to the Pacific ocean, *Chem. Oceanogr., 10*, 15–49, 1990.

Merrill, J. T., R. E. Newell, and A. S. Bachmeier, A meteorological overview for the Pacific Exploratory Mission-West Phase B, *J. Geophys. Res., 102*, 28,241–28,253, 1997.

Molod, A., H. M. Helfand, and L. L. Takacs, The climatology of parameterized physical processes in the GEOS-1 GCM and their impact on the GEOS-1 data assimilation system, *J. Climate, 9*, 764–785, 1996.

Moore, H. E., S. E. Poet, and E. A. Martell, ^{222}Rn, ^{210}Pb, ^{210}Bi, and ^{210}Po profiles and aerosol residence times versus altitude, *J. Geophys. Res.*, *78*, 7065–7075, 1973.

Moorthi, S., and M. J. Suarez, Relaxed Arakawa-Schubert: A parameterization of moist convection for general circulation models, *Mon. Weather Rev.*, *120*, 978–1002, 1992.

Nazaroff, W. W., Radon transport from soil to air, *Rev. Geophys.*, *30*, 137–160, 1992.

O'Brien, K., A. De La Zerda Lerner, M. A. Shea, and D. F. Smart, The production of cosmogenic isotopes in the Earth's atmosphere and their inventories, in *The Sun in Time*, pp. 317–342, Univ. of Ariz. Press, Tucson, 1991.

Ogura, Y., and H. -R. Cho, Diagnostic determination of cumulus cloud populations from observed large-scale variables, *J. Atmos. Sci.*, *30*, 1276–1286, 1973.

Ogura, Y., and T. Takahashi, Numerical simulation of the life cycle of a thunderstorm cell, *Mon. Weather Rev.*, *99*, 895–911, 1971.

Palmer, P. I., D. J. Jacob, K. Chance, R. V. Martin, R. J. D. Spurr, T. P. Kurosu, I. Bey, R. Yantosca, A. Fiore, and Q. Li, Air mass factor formulation for spectroscopic measurements from satellites: Application to formaldehyde retrievals from GOME, *J. Geophys. Res.*, in press, 2001.

Penner, J. E., R. J. Charlson, J. M. Hales, N. S. Laulainen, R. Leifer, T. Novakov, J. Ogren, L. F. Radke, S. E. Schwartz, and L. Travis, Quantifying and minimizing uncertainty of climate forcing by anthropogenic aerosols, *Bull. Am. Meteorol. Soc.*, *75*, 375–400, 1994.

Preiss, N., M.-A. Melieres, and M. Pourchet, A compilation of data on lead 210 concentration in surface air and fluxes at the air-surface and water-sediment interfaces, *J. Geophys. Res.*, *101*, 28,847–28,862, 1996.

Rangarajan, C., and S. Gopalakrishnan, Seasonal variation of beryllium-7 relative to caesium-137 in surface air at tropical and sub-tropical latitudes, *Tellus*, *22*, 115–120, 1970.

Rasch, P. J., et al., A comparison of scavenging and deposition processes in global models: Results from the WCRP Cambridge workshop of 1995, *Tellus, Ser. B*, *52*, 1025–1056, 2000.

Rehfeld, S., and M. Heimann, Three-dimensional atmospheric transport simulation of the radioactive tracers ^{210}Pb, ^{7}Be, ^{10}Be, and ^{90}Sr, *J. Geophys. Res.*, *100*, 26,141–26,161, 1995.

Sanak, J., A. Gaudry, and G. Lambert, Size distribution of ^{210}Pb aerosols over oceans, *Geophys. Res. Lett.*, *8*, 1067–1069, 1981.

Sanak, J., G. Lambert, and B. Ardouin, Measurements of stratosphere-troposphere exchange in Antarctica by using short-lived cosmonuclides, *Tellus, Ser. B*, *37*, 109–115, 1985.

Schery, S. D., S. Whittlestone, K. P. Hart, and S. E. Hill, The flux of radon and thoron from Australian soils, *J. Geophys. Res.*, *94*, 8567–8576, 1989.

Schubert, S. D., and R. B. Rood, Proceedings of the workshop on the GEOS-1 five-year assimilation, *NASA Tech. Mem. 104606*, *7*, 1995.

Schubert, S. D., R. B. Rood, and J. Pfaendtner, An assimilated data set for Earth Science applications, *Bull. Am. Meteorol. Soc.*, *74*, 2331–2342, 1993.

Singh, H., et al., Distribution and fate of select oxygenated organic species in the troposphere and lower stratosphere over the Atlantic, *J. Geophys. Res.*, *105*, 3795–3806, 2000.

Stoller, P., et al., Measurements of atmospheric layers from the NASA DC-8 and P-3B aircraft during PEM-Tropics A, *J. Geophys. Res.*, *104*, 5745–5764, 1999.

Strom, J., B. Strauss, T. Anderson, F. Schroder, J. Heintzenberg, and P. Wendling, In situ observations of the microphysical properties of young cirrus clouds, *J. Atmos. Sci.*, *54*, 2542–2553, 1997.

Takacs, L. L., A. Molod, and T. Wang, Documentation of the Goddard Earth Observing System (GEOS) general circulation model - version 1, *NASA Tech. Memo., TM-104606*, 1, 1994.

Tiedtke, M., Representation of clouds in large-scale models, *Mon. Weather Rev.*, *121*, 3040–3061, 1993.

Turekian, K. K., Y. Nozaki, and L. K. Benninger, Geochemistry of atmospheric radon and radon products, *Annu. Rev. Earth Planet. Sci.*, *5*, 227–255, 1977.

Turekian, K. K., W. C. Graustein, and J. K. Cochran, Lead-210 in the SEAREX program: An aerosol tracer across the Pacific, in *Chemical Oceanography*, vol. 10, edited by J. P. Riley, R. Chester, and R. A. Duce, pp. 51–80, Academic, San Diego, Calif., 1989.

Uematsu, M., R. A. Duce, and J. M. Prospero, Atmosphere beryllium-7 concentrations over the Pacific Ocean, *Geophys. Res. Lett.*, *21*, 561–564, 1994.

Viezee, W., and H. B. Singh, The distribution of beryllium-7 in the troposphere: Implications on stratospheric/tropospheric air exchange, *Geophys. Res. Lett.*, *7*, 805–808, 1980.

Wesely, M. L., and B. B. Hicks, Some factors that affect the deposition rates of sulfur dioxide and similar gases on vegetation, *J. Air Pollut. Contr. Assoc.*, *27*, 1110–1116, 1977.

Wilkening, M. H., W. E. Clements, and D. Stanley, Radon 222 flux measurements in widely separated regions, in *The Natural Radiation Environment II*, pp. 717–730, U.S. Energy and Res. Dev. Admin., Oak Ridge, Tenn., 1975.

I. Bey, D.J. Jacob, H. Liu, and R.M. Yantosca, Department of Earth and Planetary Sciences and Division of Engineering and Applied Sciences, Pierce Hall, 29 Oxford Street, Harvard University, Cambridge, MA 02138. (bey@io.harvard.edu; djj@io.harvard.edu; hyl@post.harvard.edu; bmy@io.harvard.edu)

(Received June 6, 2000; revised September 19, 2000; accepted December 14, 2000.)